AI-AEC-12857
PHYSICS

ANNUAL TECHNICAL PROGRESS REPORT

LMFBR PHYSICS PROGRAMS

GFY 1969

The preceding Quarterly Progress Report was:
AI-AEC-12815

ATOMICS INTERNATIONAL

A DIVISION OF NORTH AMERICAN ROCKWELL CORPORATION

CONTRACT: AT(04-3)-701
ISSUED: SEPTEMBER 30, 1969

DISCLAIMER

DISTRIBUTION

This report has been distributed according to the category "Physics" as given in the Standard Distribution for Unclassified Scientific and Technical Reports, TID-4500.

CONTENTS

Program:	Civilian Power, LMFBR		
AEC Task:	5-B, Reactor Physics, Fast Reactor Physics Experiments		
Project Manager:	H. A. Morewitz		
Reporting Period:	Fiscal Year 1969		
General Order: 7701	Subaccount: 14610	AEC Category: 04-01-61-02.1	

Principal Investigators: T. H. Springer, R. J. Tuttle, H. N. Royden

I. PROJECT OBJECTIVES

The objectives of this project are to (a) determine reactivity, temperature, and Doppler coefficients of various materials in a variety of fast reactor spectra; (b) investigate effects due to different geometric arrangements of such materials, including the variation of the surface-to-mass ratio; (c) provide experimental results for the purpose of checking theoretical predictions; and (d) develop improved experimental and theoretical methods for treatment of problems in the field of fast reactor physics.

II. TECHNICAL PROGRESS DURING FISCAL YEAR 1969

Research at the ECEL this year has concentrated on reactor compositions and spectra typical of current LMFBR designs. This concentration has permitted the detailed investigation of some of the present difficult problems in fast reactor development, such as the reactivity of pin-clusters of absorbers, the reactivity of strongly self-shielded absorbers, and the reactivity of individual plutonium isotopes. Experimental and calculational techniques have been studied and refined, leading to a better understanding of existing and potential capabilities for resolving these problems.

The first of the three cores (Core 17) studied this year was a plate-type test region simulating a typical LMFBR. This test region was composed of fully enriched uranium, natural uranium, carbon, metallic sodium, stainless steel, and aluminum. The central U^{235}/U^{238} median fission energy (mfe) was 93 kev which is equivalent to 160 kev for a plutonium fueled core. This core was modified by installing boxes of fuel pins (Figure 1) to form a central subzone of FBR-type fuel elements (Figure 2). This core was identified as 17P

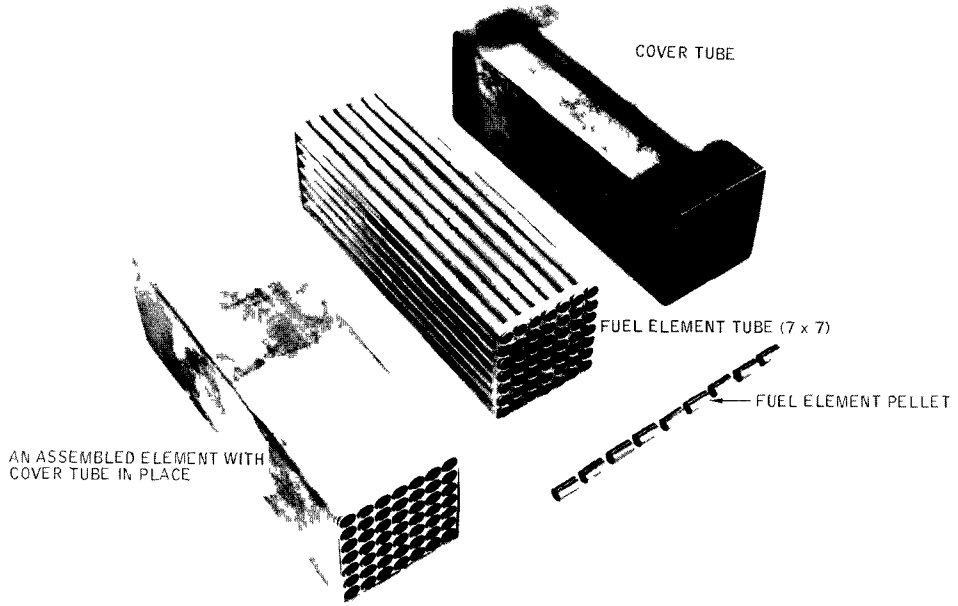

Figure 1. Fuel Pin Boxes

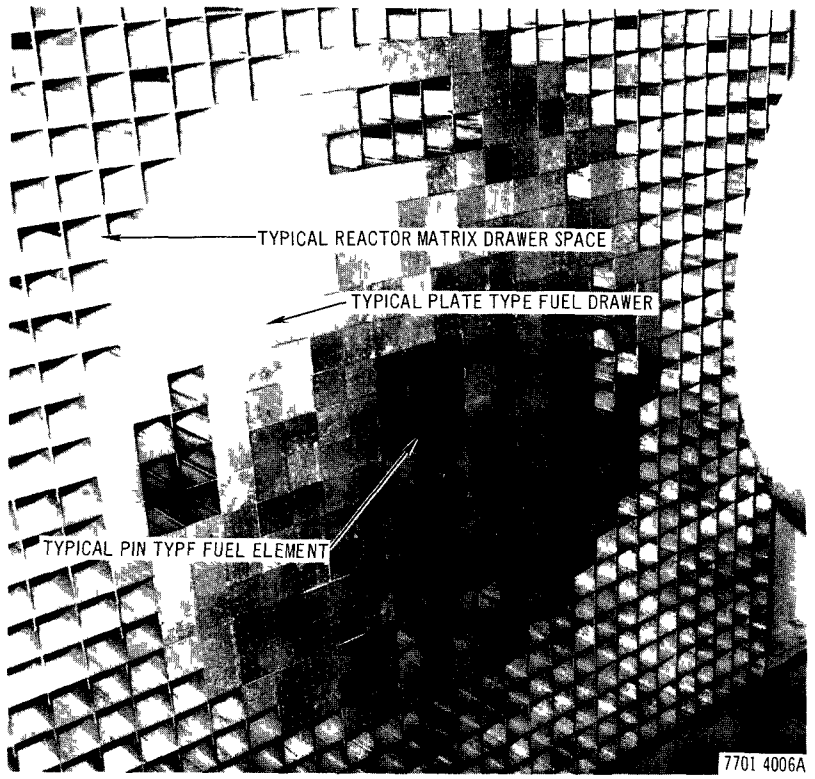

Figure 2. Central Subzone of FBR-Type Fuel Elements

and had a central U^{235}/U^{238} mfe of 69 kev. Core 18 was formed by reloading the test region of Core 17, but using empty sodium cans to produce a spectrum typical of a voided LMFBR. This core had a central U^{235}/U^{238} mfe of 125 kev.

A. REACTIVITY MEASUREMENTS

The central reactivity worths of a wide variety of sample materials with extensive surface-to-mass variations were measured in these cores. The results of these measurements are summarized in Table 1. Some control rod materials were investigated in considerable detail because of their particular interest to LMFBR development.

Present design concepts of control rods include massive tantalum rods and thick boron carbide as favored alternates. Because of tantalum's strong resonance absorption and the thick sections involved in present conceptual control rod designs, tantalum control rods are strongly self-shielded. Calculated results of the reactivity worth of these rods are subject to considerable uncertainty. To provide a sensitive test of calculational methods, the reactivity worths of tantalum samples covering a wide range of self-shielding were measured in Core 17. The results of these measurements are shown in Figure 3, where the specific worth is plotted against the atomic thickness, $N\ell$. (N is the atomic density, ℓ is the mean chord length of the sample.) The extremes in self-shielding were obtained with a tube (0.001-in. thick wall) for nearly infinite dilution and a 1.75-in. diameter cylinder for the thickest sample. The thickest sample is more self-shielded than some current control rod designs; therefore, the reactivity of such rods may be based on interpolation within the measured data, rather than by extrapolation from thin samples.

All but the largest sample were measured using the reactivity oscillator technique; the largest sample, however, could not be oscillated because of its size. The reactivity of this sample, relative to a void, was measured by a modification of the period method. The reactivity of the reactor was determined for a reproducible configuration, with the sample in place at the center and with it removed, by means of the dynamic reactivity or inverse-kinetics analysis. Repetitive closure of the split-table reactor showed that this movement had a negligible effect on the measured reactivity. The accuracy in these measurements, ±0.05 cents, was limited by the temperature coefficient of the reactor

TABLE I

SPECIFIC REACTIVITY

Material	Mass (gm)	Reactivity (10^{-3} ¢/gm) Core No. 17	17P	18
Scattering Materials				
Polyethylene	1.5056	+54.79 ± 0.33	-	-
	6.2740	+61.659 ± 0.077	-	-
Li^7	0.2935	-1.19 ± 0.95	-	-
	1.6891	-2.89 ± 0.16	-	-
	3.8466	-0.715 ± 0.125	-	-
C	5.5404	-0.0063 ± 0.0088	-	-
	16.2330	-0.031 ± 0.022	-	-
	17.0468	-	-0.154 ± 0.021	-0.456 ± 0.018
Na	0.5524	+1.10 ± 0.52	-	+0.31 ± 0.52
	3.2599	-1.36 ± 0.089	-	-1.21 ± 0.09
	6.8432	-0.094 ± 0.069	-0.218 ± 0.053	-0.172 ± 0.042
Mg	17.0835	-0.458 ± 0.020	-	-
Al	26.3802	-0.436 ± 0.018	-0.326 ± 0.015	-0.478 ± 0.011
Lavite	23.3595	-0.303 ± 0.015	-	-
Pb	110.5786	-0.0873 ± 0.0032	-	-
Bi	39.7364	-0.080 ± 0.011	-	-
Structure and Control				
Li^6	0.2887	-172.84 ± 0.87	-	-
	1.6350	-176.51 ± 0.18	-	-
	3.1350	-172.33 ± 0.12	-	-
B/Bi	0.6398(B)	-49.92 ± 0.50	-	-
	0.8245(B)	-50.60 ± 0.52	-	-
B	3.3671	-53.42 ± 0.14	-	-
	4.1098	-52.38 ± 0.11	-	-
	5.1237	-52.85 ± 0.09	-	-
B_4C	9.9186	-48.07 ± 0.06	-	-
B^{10}	6.3650	-43.20 ± 0.01	-	-
W	188.4561	-1.3061 ± 0.0018	-	-
Nb	84.9437	-2.0836 ± 0.0040	-	-

(Continued)

TABLE 1

SPECIFIC REACTIVITY
(Sheet 2)

Material	Mass (gm)	Reactivity (10^{-3} ¢/gm) Core No. 17	Core No. 17P	Core No. 18
Structure and Control				
Stainless Steel (304)	77.8543	-0.3578 ± 0.0033	-0.3045 ± 0.0045	-0.3561 ± 0.0039
Inconel-600	6.9630	-0.513 ± 0.069	-	-0.636 ± 0.046
Inconel-750	81.5572	-	-0.4085 ± 0.0043	-0.4653 ± 0.0037
Ta	1.5563	-5.87 ± 0.18	-6.25 ± 0.20	-
	12.8422	-4.393 ± 0.024	-	-
	53.5927	-3.9554 ± 0.0063	-	-
	163.2689	-3.6102 ± 0.0029	-3.5968 ± 0.0021	-3.1090 ± 0.0020
Fuel Materials				
PuO_2 No. 2	66.1960	+12.999 ± 0.010	+12.071 ± 0.005	+12.618 ± 0.007
No. 4	66.1916	+13.039 ± 0.011	+12.084 ± 0.006	+12.654 ± 0.005
No. 5	66.1871	+13.038 ± 0.011	-	-
No. 6	61.8518	+09.632 ± 0.019	-	+9.398 ± 0.014
No. 7	31.370	+10.265 ± 0.027	-	-
No. 9	62.0718	+08.161 ± 0.020	-	+7.924 ± 0.014
U^{235}	4.0081	+10.667 ± 0.091	-	-
	13.7821	+11.165 ± 0.026	-	-
	117.6789	+11.1700 ± 0.0031	+10.7368 ± 0.0032	-
	183.3159	+11.2433 ± 0.0020	+10.7796 ± 0.0020	+10.6802 ± 0.0019
Fertile Materials				
U^{238}	59.9856	-0.7919 ± 0.0058	-	-
	117.8490	-0.8103 ± 0.0029	-	-
	184.7387	-0.8049 ± 0.0026	-0.8360 ± 0.0019	-0.7000 ± 0.0016
$U^{238}O_2$	78.8523	-0.7518 ± 0.0038	-0.7886 ± 0.0042	-0.7747 ± 0.0038
Th	114.0429	-1.5439 ± 0.0030	-	-

The isotopic compositions of these samples (within experimental uncertainties) are:

	239	240	241	242
No. 2, 4, 5	0.914	0.079	0.007	0.004
No. 7	0.843	0.133	0.020	0.004
No. 9	0.407	0.419	0.103	0.068

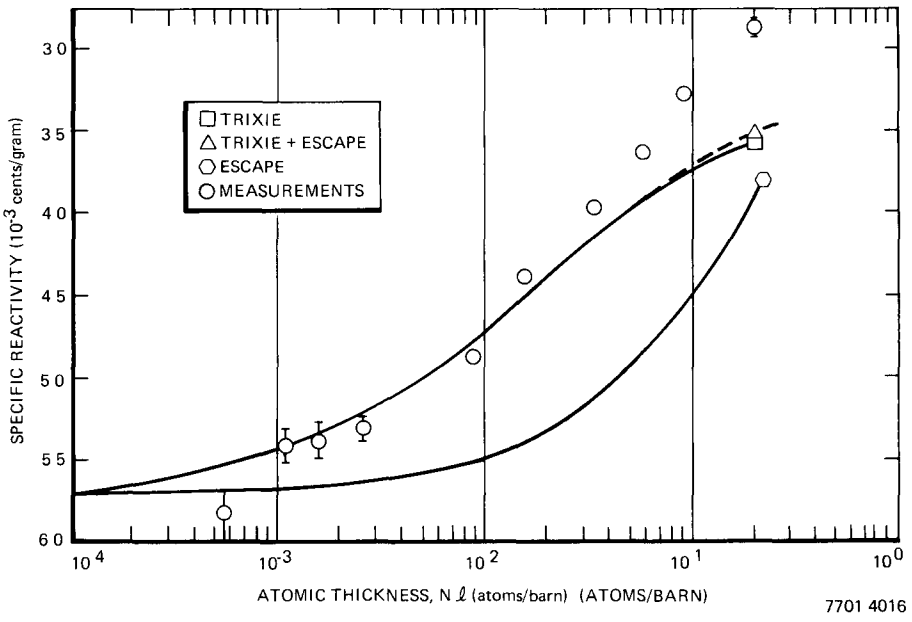

Figure 3. Specific Reactivity of Tantalum in ECEL 17

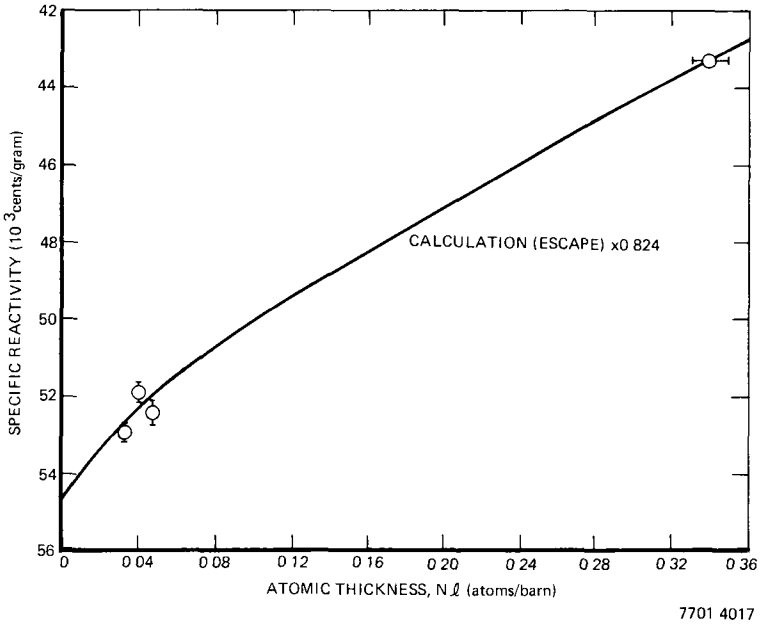

Figure 4. Specific Reactivity of Boron in ECEL 17

as the power approached 150 watts during each of several period determinations. Refinement of this technique will permit reactivity measurements of large samples with even smaller uncertainty than that in these measurements.

Analysis and interpretation of reactivity measurements with clusters of pins requires knowledge of the mean chord length. For compact samples, this can be determined from the ratio of the volume to an appropriate "rubber-band" surface. For open clusters, however, this approach is unsatisfactory. Modification of a portion of a Monte Carlo program has produced a computer code, MCL, that can calculate the mean chord length for any sample with cylindrical symmetry. This code is directly applicable to reactivity calculations of LMFBR control rods and calculation of the gamma-ray absorption of such rods.

Three sets of calculations are shown for comparison with the measured values. The calculations were done with first-order perturbation theory using cross-sections modified by TRIXIE (a resonance cross-section code), by ESCAPE (a smooth cross-section code), and by a combination of the two in which ESCAPE is used for cross-sections above the upper energy limit of the resonance data. The TRIXIE calculations show good agreement with the measurements for dilute samples, but for thick samples the calculations deviate progressively from the measurements as the self-shielding increases. It is expected that this deviation will be eliminated by using exact perturbation theory, in which the unperturbed real flux and perturbed adjoint flux are used. This calculation is underway.

The reactivity worth of boron was also measured as a function of self-shielding in Core 17. These results are shown in Figure 4. The samples were composed of powdered natural boron or enriched boron-10 encapsulated within stainless steel or aluminum cans. The dimensions of the boron samples were determined by neutron radiography. The calculated variation of specific reactivity was obtained by first-order perturbation theory using effective cross sections based on the escape probability method. The real and adjoint fluxes used in this calculation were produced by the diffusion theory code CAESAR. Use of the calculated value of beta-effective, 0.00748, to convert the calculated reactivity to cents yielded values in severe disagreement with the experiment. The good agreement shown in the figure was achieved only by multiplying the converted calculated values by a normalization factor, A = 0.824.

A small adjustment was required by the natural boron samples to account for moderation of neutrons in the sample by the boron-11. This moderation makes the samples more negative in reactivity because of the increased absorption probability for the moderated neutrons and the slightly lower importance of the moderated neutrons that escape. Each of these effects accounted for about 1% of the observed reactivity. Scattering effects were negligible for the thickest sample, which was composed of enriched boron-10.

In order to check further the discrepancy between those measured and calculated absolute reactivity worths which required use of an arbitrary normalization factor, the reactivity of lithium-6 was calculated by using the escape probability method. The escape probability method is applicable only for samples with slowly varying cross sections. Both lithium-6 and boron-10 are well suited to this limitation. For this isotope, the normalization factor, A, was found to be 0.796. Thus, the calculations overestimate reactivity for these simple absorbers by a factor of about 1.23. This factor agrees with results obtained at this laboratory over the last eight years and is in agreement with comparisons made at several other laboratories.

Possible causes of this discrepancy, such as a systematic error in delayed neutron yields, are being investigated in a company-sponsored project. If the recent values for delayed neutron yields reported by Masters, et al, of Los Alamos are used, the value of beta-effective changes from 0.00748 (using Keepins values for delayed-neutron fractions) to approximately 0.00844. This change reduces the discrepancy from 1.23 to 1.10.

The specific reactivities of scattering materials do not show any simple correlation with sample size as is observed with absorbers. This is apparent from comparisons of the several lithium, sodium, carbon, and polyethylene samples listed in Table 1. Some peculiar results requiring rejection of the data also occurred in measurements with boron carbide and boron mixed with bismuth. The cause of this erratic behavior is unclear at this time. In polyethylene, it is quite likely a simple size effect resulting from multiple scattering by hydrogen. While the possibility of an experimental artifact, such as variable amounts of absorbed water or oxides, cannot be definitely excluded from the other samples, the erratic results in such dissimilar samples as carbon and sodium argues against the existence of a common cause of such an artifact. A possible cause

TABLE 2

DERIVED SPECIFIC REACTIVITY OF OXYGEN

Sample Pairs	Specific Reactivity (10^{-3} ¢/gm O_2)
Al-Al_2O_3 No. 1	-0.308 ± 0.030
Al-Al_2O_3 No. 2	-0.366 ± 0.066
Al-Al_2O_3 No. 3	-0.270 ± 0.023
Pb-PbO	-0.52 ± 0.12
Pb-PbO_2	-0.346 ± 0.069
Mg-MgO No. 1	+4.402 ± 0.072
Mg-MgO No. 2	+3.79 ± 0.35

of this behavior may be interference between fine structure in the real and adjoint fluxes, introduced in varying amounts by moderation in these light scatterers. Single, double, and triple scatters may produce interference by different amounts, thus causing an irregular variation in reactivity with sample size.

Problems of the above type complicate the measurement of the reactivity worth of oxygen, for example, when the technique whereby the reactivity difference between some metal and its oxide is employed. A variety of metal-oxide pairs have been used in an attempt to clarify this difficulty but this has not been completely successful. The results of these measurements are shown in Table 2. A value of -0.295×10^{-3} ¢/gm has been taken for the worth of oxygen in Core 17 by excluding the positive values.

Several clusters of pins of $U^{238}O_2$ and of Ta with different pin pitches have been used to determine the reactivity effects of pin spacing. The pin diameter and spacings were chosen to approximate current fuel element designs. Samples with 1, 4, and 7 tantalum pins were measured. The effect of filling the spaces between the tantalum pins with NaF was also measured. These results have not yet been completely analyzed.

A preliminary evaluation of the reactivity worths of the individual higher isotopes of Pu has been conducted for Core 16, a U^{235}/U^{238} fueled assembly with a test region median fission energy of 66.4 kev. The reactivity worths of

four samples, each with a different ratio of Pu^{239} to Pu^{240} to Pu^{241} to Pu^{242}, were determined and used to derive, by means of four simultaneous equations, the specific reactivity worths of each isotope individually. Since the self-shielding factors for each isotope vary from one sample to the next, the specific worth values listed below are only approximate, but may serve to provide some indication of relative magnitudes for the first three isotopes.

Pu Isotope	Specific Worth (10^{-3} ¢/gm)	
	Measured*	Calculated†
239	+15.6	+17.8
240	-4.6	-0.1
241	+21.0	+24.8
242	+31.1	+1.1

*Self-shielded
†At infinite dilution

The measured specific worth of Pu^{242} is expected to be too large since, relative to Pu^{239}, it is always very dilute; however, one would not predict it to be more positive than Pu^{239} or Pu^{241}. When the self-shielding factors are applied, this difficulty may be clarified.

Inasmuch as the calculated absolute values for the reactivity worths of the fissionable isotopes are consistently found to be too high in fast reactor spectra as is seen here, it is informative to investigate the ratio of the calculated to the experimental values of reactivity of Pu^{241} and Pu^{239}. The agreement is remarkably good, the ratio of Pu^{241} to Pu^{239} being 1.35 experimentally and 1.39 analytically.

B. DOPPLER-EFFECT MEASUREMENTS

The temperature coefficients of reactivity of a variety of samples have been measured in the three cores. Some of the results of measurements for Cores 17 and 17P with the standard-sized samples are shown in Table 3. In addition to the standard measurements, a series of measurements made while using heated blankets was done to investigate the effect of the reactor temperature on the

TABLE 3

DOPPLER-EFFECT MEASUREMENTS

Sample	Doppler Effect		Temperature Interval (°C)
	Core No.		
	17	17P	
Ta	-0.0365 ± 0.0006	-0.0357 ± 0.0006	25 to 600
U^{238}	-0.0105 ± 0.0006	-0.0091 ± 0.0006	25 to 600
$U^{235}O_2$	-0.0032 ± 0.0008	-0.0047 ± 0.0008	25 to 810

TABLE 4

EFFECT OF HEATED BLANKET ON SMALL-SAMPLE TEMPERATURE COEFFICIENT

Sample	Blanket	C_{hb}/C_{cb}
Th	Th	0.81
Th	U^{238}	1.00
U^{238}	Th	0.96
U^{238}	U^{235}	0.99
U^{238}	U^{238}	0.85

*Ratio of coefficient in heated blanket to that in cold blanket

observed Doppler effect of a small sample. This problem is of considerable significance in the application of small sample measurements to analysis of full size reactors. The interpretation of these measurements is based on the assumption that the interaction between a heated sample and a cold reactor is close to that obtained when both sample and reactor are at approximately the same temperature. This has been investigated by surrounding the sample location at the center of the reactor by a massive blanket that can be electrically heated. The samples used were Th and U^{238} in blankets of Th, U^{235}, or U^{238}. The blanket was either at room temperature or heated to 400°C. Only when the heavy absorber in the sample and in the blanket were the same, was there any dependence on blanket temperature. These results are shown in Table 4. This effect was a general

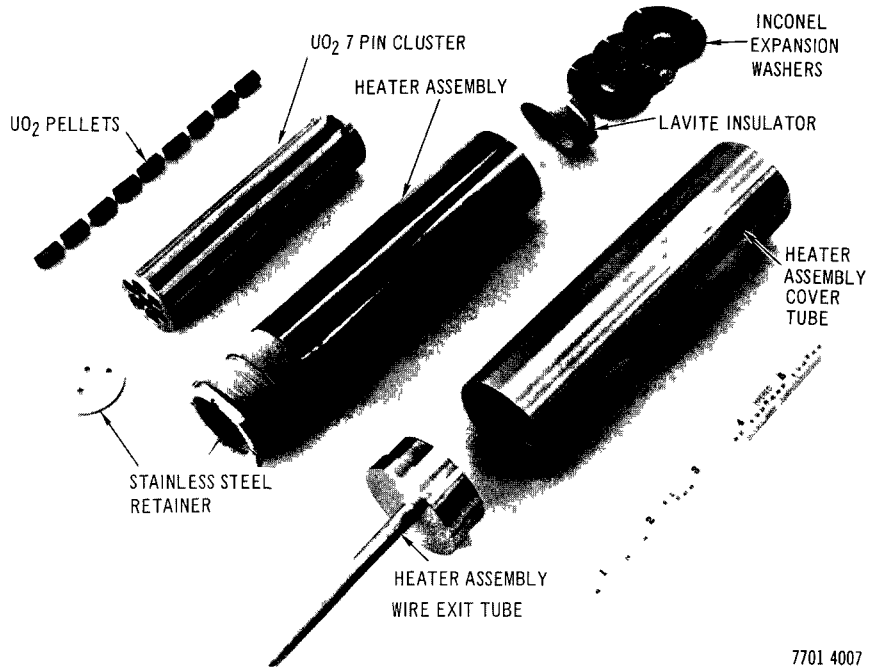

Figure 5. Sample Construction

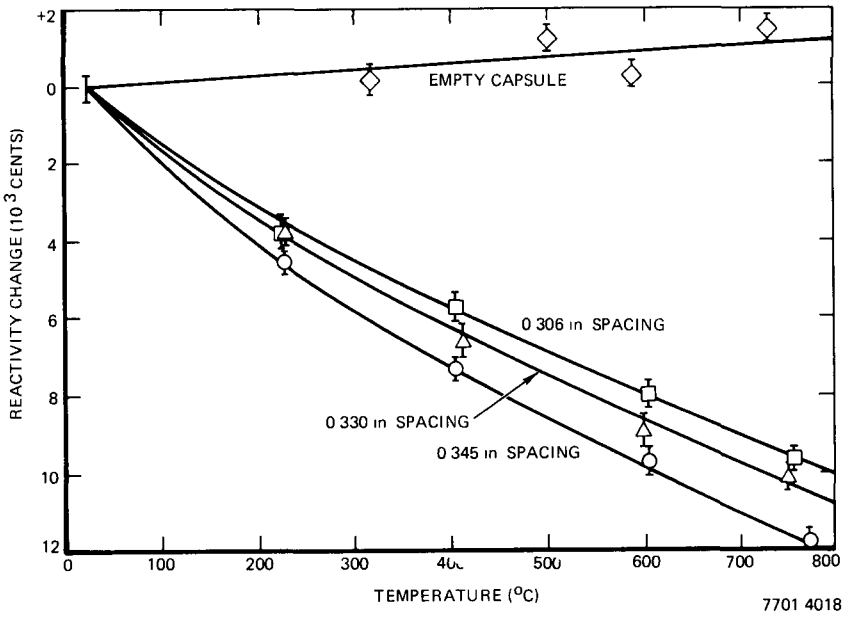

Figure 6. Temperature Coefficients of Seven-Pin Clusters of $U^{238}O_2$ in ECEL 17

reduction by about 17% in the magnitude of the Doppler reactivity change. This may be taken as an approximate upper limit since it is produced by a concentrated single isotope, whereas material is distributed in a more nearly homogeneous arrangement in the actual reactor.

Measurements were also made with clusters of $U^{238}O_2$ with varying pitch spacings. The construction of one of these samples is shown in Figure 5. The results of these measurements are shown in Figure 6 and are listed in Table 5. The preliminary calculations do not show good agreement with experiment as far as the Doppler effect is concerned. Refinements are being worked out.

C. SPECTRUM MEASUREMENTS

In order to provide direct differential spectra for comparison with calculations, measurements were made in each of the cores with proton-recoil proportional counters. These measurements are described in detail in the Reactor Physics Measurements Annual Report. The calculated central flux spectra are compared with the measurements in Figures 7, 8, and 9. Both coarse-group spectra calculated by CAESAR, a diffusion theory code, and fine-group spectra calculated by AILMOE are shown. The AILMOE spectra have been smoothed by means of a Gaussian resolution function to make the calculations more directly comparable to the measured spectra.

Because of the small size of the subzone in Core 17P, AILMOE, which does a fundamental mode calculation, is not directly applicable; therefore, a smooth, pointwise adjustment of the AILMOE spectrum was made to produce a fine group spectrum with the same integrated flux in each coarse-energy group interval as exists in the CAESAR calculation.

Activation foils were irradiated in Core 18, but the data have not yet been analyzed.

D. ANALYTICAL STUDIES

The resonance self-shielding code TRIX has been improved significantly, and now provides modified cross sections that predict reactivity effects with considerable accuracy. In particular, comparisons of U^{238} cross sections calculated by TRIX with optical-model calculations have led to a more accurate method for accounting for different angular momenta neutrons.

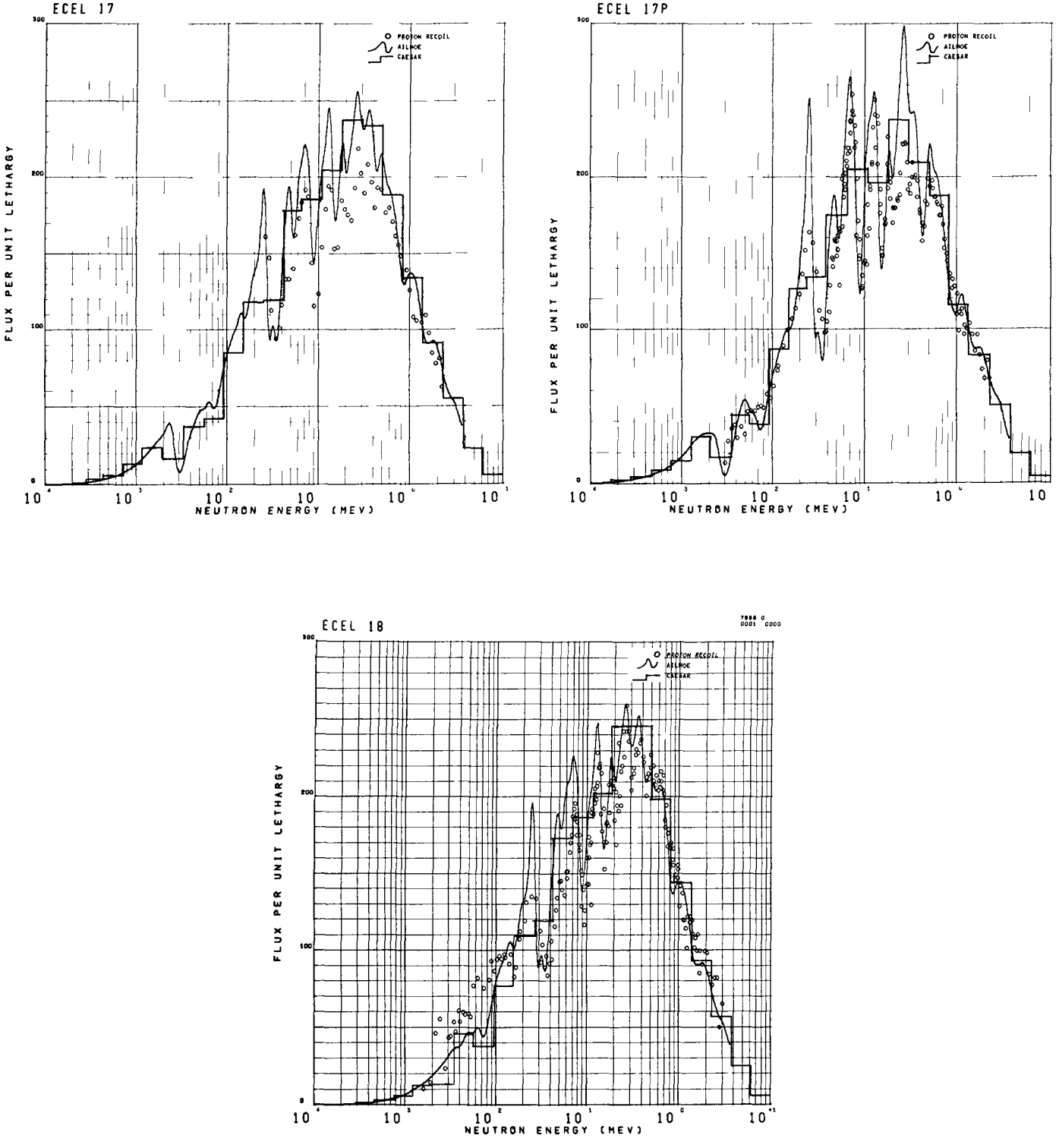

7701-4019

Figures 7, 8, and 9. ECEL Neutron Flux Spectra

TABLE 5

MEASUREMENTS WITH 7 PIN CLUSTERS OF $U^{238}O_2$

$[\rho(T) = A + BT(k)^{1-\gamma}]$

Pin Spacing (in.)	Mass $U^{238}O_2$ (gm)	ρ (¢)	$\Delta\rho$ (300-1100°K)	$\left\|\frac{1}{\rho}\right\| \frac{d\rho}{dT}$ (300-1100°K) (x 10^{-4})	A	B	γ
0.345	164.48	-0.13474 ±0.00062	-0.01356 ±0.00013	-1.258 ±0.013	0.1543	-0.0146	0.8
0.330	164.48	-0.13487 ±0.00061	-0.01275 ±0.00015	-1.182 ±0.015	2.1262	-0.00191	0.6
0.306	164.48	-0.13307 ±0.00060	-0.01129 ±0.00018	-1.060 ±0.018	0.1278	-0.00169	0.6
0.395*	78.85	-0.05947 ±0.00034	-0.00859 ±0.00041	-1.806 ±0.055	0.2568	-0.0350	0.9

*Single rod diameter (in.)

TABLE 6

CALCULATED AND MEASURED SPECIFIC REACTIVITY OF TANTALUM*

Core No.	mfe (kev)	Reactivity (10^{-3} ¢/gm)		Difference (%)
		Calculation	Experiment	
14	3.9	-8.05	-7.79	-3.3
15	17.8	-5.21	-5.02	-3.8
16	66.4	-4.18	-3.81	-9.7
17	93.	-3.87	-3.61	-7.2

*Sample is 0.438 in. diameter by 4.0 in. long

Calculations of tantalum reactivity worths for several cores are now in good agreement with the measurements. The results of this comparison for a particular sample size are shown in Table 6.

Detailed analyses of several methods for measuring the effective capture-to-fission ratio have been conducted and are partially complete. The methods under consideration are those of Feiner ("Reactor Physics in the Resonance and Thermal Regions," Vol. II, 1966, MIT Press), Redman and Bretscher (Nucl. Sci. Eng. 27, 34 (1967), and Carpenter (based on direct measurement of the normalization integral in the perturbation equation). An additional, relative, method proposed by Springer can be used to test the consistency of results by the other methods. Preliminary results have been sent to interested persons at ANL-Lemont and AB Atomenergi.

Feiner's method involves the measurement of reaction rates and reactivity worths of the fissile sample and an absorber. The formula for $\bar{\alpha}$ can be schematically represented as

$$\bar{\alpha} = (\nu A - BX)C \quad ,$$

where ν is the average number of neutrons per fission; X is an experimental ratio; and the terms A, B, and C are calculated correction terms that are related to the ratio of the high energy neutron importance to the low energy neutron importance. This relation causes a correlation in the three calculated terms; consequently, a change in importance which tends to increase A will decrease B and increase C, thus implying a higher value for $\bar{\alpha}$. The correlation has further ramifications, however, because such a change in importance can be produced by increasing $\bar{\alpha}$ in the calculations used to generate the correction terms for the measurement. Whether this process, if pursued iteratively, would converge or diverge has not yet been investigated. It is concluded that Feiner's method, in its present form, with heavy reliance on calculations, is not suitable for measurements of $\bar{\alpha}$ in fast reactors.

The other two absolute methods use neutron sources as part of the determination of the importance of neutrons. It appears possible to use a combination of sources and absorbers to reduce both random and systematic errors in these methods. Study of these methods is continuing.

A cross section library has been prepared for use with the transport-theory code ANISN. Some preliminary calculations have been performed for comparison with the diffusion-theory code CAESAR. As a test case, an infinite reactor with the same composition as the test region of Core 17 was calculated by using both codes. All comparable results were essentially identical. A calculation of Core 17 with ANISN (S_8) gave an eigenvalue about 4.5% greater than that calculated for the same configuration by CAESAR. This discrepancy is probably caused by the assignment of two different thorium cross-section sets to the inner and outer parts of the decoupler. The boundary between the two parts is used, somewhat arbitrarily, to adjust the calculated eigenvalue. This procedure will also be tried with ANISN.

E. REACTOR DESIGN AND CORE MATERIALS

Preliminary designs for Core 19 have been completed. This core will be a cylindrical reactor with a complete axial test region surrounded by decoupler, driver, and reflector regions as in the present spherical reactor. The test region will have axial reflectors to provide simulation of the central part of an LMFBR. The core will be loaded with plate materials.

Detailed mechanical designs have been completed for Core 20, which will have a test region loaded with simulated LMFBR fuel elements. These elements will have oxide pellets of suitable diameter loaded into stainless steel tubes in sodium-filled fuel cans. Individual elements will be removable to permit investigation of control rods and fuel element modifications. A large quantity of surplus U-Al alloy fuel element material used on another program has been modified for use at the ECEL. Some of this material was punched into discs for use in the pin-type fuel elements in Core 17P. Additional material is being formed into plates for use as driver region fuel in the cylindrical cores.

III. EVALUATION OF EFFORT DURING FISCAL YEAR 1969

A variety of materials pertinent to the LMFBR development effort and to measurements in fast reactor physics was used in reactivity, temperature, and Doppler coefficient measurements. The core compositions were directly related to the LMFBR; one representing normal operation, another being the same

core with the sodium removed, and a third simulating the detailed geometry of a pin-fueled reactor.

The effect of geometry on reactivity and temperature coefficients was investigated not only by means of an exceptionally wide range of surface-to-mass ratios for tantalum, but by using various clusters of small diameter pins.

The wide range of tantalum measurements has provided a stringent test for reactivity calculations. Comparison of measured boron reactivities with normalized calculations showed the existence of minor reactivity effects due to scattering.

The changes in the spectrum fine structure in these cores provided information for the further development of the proton-recoil spectrum measurements and their comparison with calculations.

The measurement of the reactivity worth of a large tantalum sample established the ability to make highly precise measurements with samples, or reactor configurations, that are not amenable to the reactivity oscillator.

Analyses of methods for measuring the effective capture-to-fission ratio have shown some difficulties with current methods and indicate modifications to improve them.

The calculation of reactivity worths for open clusters of pins, for which simple surface-to-mass relations fail, has been facilitated by development of an exact method. This method is directly applicable to certain LMFBR control rod designs.

Several modifications of the TRIX code were made to improve the accuracy of calculated cross sections and Doppler effects at high energies. A better value of the radius of the centrifugal potential (used in calculating penetrabilities of neutrons with nonzero angular momenta, ℓ) reduced U^{238} cross-sections by up to 20% in the range of energy up to 100 kev. Allowing elastic scattering to permitted states with nonincident values of ℓ reduced the Pu^{239} capture cross-section by up to 2% in the range of energy up to 100 kev. Introduction of an energy dependent potential scattering cross section for the resonance absorber, including interference between resonance and potential scattering, changed effective cross-sections. For U^{238} in a typical fast breeder reactor, cross-sections decreased by as much as 2% in the energy range up to 100 kev due to this new

potential scattering cross-section. They increased, however, by about 4% at 10 kev and 20% at 100 kev due to the high energy interference term. Self-shielding of the scattering cross-sections of U^{238} in a typical FBR reduced the cross sections by about 1% at 50 kev, 15% at 10 kev, and 50% at 1 kev from infinitely dilute values. Allowing for depletion of the group flux by unresolved resonances increased the cross sections about 2% at 5 kev for the same case. Accounting for competition with inelastic scattering which has a threshold of 45 kev in U^{238} reduced the capture cross section by 40% at 100 kev. A careful comparison of U^{238} infinitely dilute cross-sections calculated with TRIX was made to optical model calculations. The agreement is within 5% to 65 kev. At high energies, TRIX values fall below optical model values, being 13% low at 100 kev. Revision of the coding including use of disc storage has reduced the IBM 360/50 machine time per run by about two minutes. (Typical case times are 2 to 6 min.)

In view of the apparent consistent deviation between calculated and measured reactivity worths, the good agreement in this case may be fortuitous and possibly misleading. Additional analytical work needs to be done to clarify this problem.

Program:	Reactor Development
AEC Task:	5-E, Monte Carlo Methods
Project Manager:	H. A. Morewitz
Reporting Period:	Fiscal Year 1969
General Order: 7701	Subaccount: 14320 AEC Category: 04-01-61-02.1

Principal Scientists: L. B. Levitt, J. Spanier

I. PROJECT OBJECTIVES

The objectives of this project are to perform the necessary research and development of Monte Carlo methods which will lead to the solution of fast reactor physics and safety problems not solvable by less accurate methods. These objectives include the development of Monte Carlo criticality and reactor analysis codes, the development of sophisticated Monte Carlo techniques which permit accurate evaluation of local effects in reactor safety studies and in experiments involving test capsules, the refinement of correlation techniques to reduce variance in parameter studies and Doppler coefficient evaluation, and the investigation and refinement of optimization of Monte Carlo estimators (in the reactor analysis codes) for variance reduction purposes (computer computation cost is proportional to the variance).

The purpose of this project is to develop Monte Carlo analysis codes which are reliable, easy to use, and cost effective on the appropriate computer systems.

II. TECHNICAL PROGRESS DURING FISCAL YEAR 1969

A preliminary version of VIM for fast critical assemblies was completed, and a detailed checkout of procedures was initiated by using ZPR-3-48 as a test model. The completed work on VIM includes the geometric description of plate-drawer type assemblies, particle tracking routines for plate-drawer type assemblies, and the random walk description utilizing an arbitrary amount of absorption weighting for variance reduction purposes.

It also includes a preliminary version of a cross section library of sufficient detail to accurately describe ZPR-3-48. While actual values of cross

sections used are subject to change, the necessary detail has been achieved through the use of individual energy grids for angular distributions and smooth cross sections for each isotope. These data sets are stacked in singly dimensioned arrays in which the beginning and end points for each isotope are separately stored for efficient retrieval when needed.

This procedure has also been used for fission and total inelastic cross section data, for discrete level inelastic data, (n,2n) data, and evaporation model cross sections. Thresholds for these reactions will be stored and only nonzero data will actually be packed in the high speed computer core.

By this elaborate and complex bookkeeping procedure, the ability to dimension the storage requirements of VIM in an optimum manner is gained. This permits the available high speed core storage to be utilized with high efficiency. The maximum amount of cross-section detail is thus made available for a given calculation without resorting to costly overlay features which would otherwise be required. The above procedure not only saves computer time and preserves maximum cross-section detail, but permits the remainder of the Monte Carlo portion of the code to be inherently simpler in structure, and thus to be easier to debug and modify when necessary.

A code, VIMB, has been written to read the ENDFB library tapes and produce data sets using one energy grid per isotope for cross-sections and one energy grid per isotope for angular distributions. The RESREG code was obtained from BNL for the purpose of generating point cross sections in the resolved energy range according to the standard ENDFB prescriptions. Data was generated by the VIMB code and was analyzed isotope by isotope with a view toward reducing the number of energy grid points without materially affecting the accuracy of reactor computations using them. A code to take the compressed data sets and place them on a VIM library tape in the final form needed for use in VIM has been written.

The elastic scattering model used in VIM permits each isotope to have its own energy grid for describing the angular distributions. The angular distributions themselves are described by tabulating, at each designated energy,

$$P_i = \frac{\int_{-1}^{\mu_i} \sigma_{el}(\mu)d\mu}{\int_{-1}^{+1} \sigma_{el}(\mu)d\mu} ,$$

where $\mu_i = -1 + 0.1\ i$ represents the cosine of the scattering angle in the C. M. system. In this way, the scattering angle is selected from the cumulative angular distribution by finding a random number

$$P_{i-1} < r < P_i \quad , \quad i = 1, \quad \ldots\ldots \ 20 \quad ,$$

and setting

$$\mu = \mu_{i-1} + \frac{r - P_{i-1}}{P_i - P_{i-1}} \times 0.1 \quad .$$

By adopting this procedure, the complexities and numerical difficulties of sampling from Legendre data are avoided. The distribution at the energy closest to the particle collision energy will be the one used. It is felt that interpolation in energy is not warranted by the present accuracy of the data and would reduce the computational efficiency of the code. This could easily be changed at a later date when either the data improves or a given calculation is thought to be particularly sensitive to this data.

The inelastic scattering model incorporates both an evaporation model and a discrete excitation level approach. The use of these two models has not been made mutually exclusive so that the total inelastic scattering cross-section at a given energy will consist of the sum of the individual excitation level cross-sections and the continuum cross-section. Present plans are to regard this scattering as isotropic in the C. M. frame.

The model for n-2n collisions used in the present version of the code allows for emergent neutron energies to be selected from two energy and temperature independent Maxwellians. Since it would be inefficient to follow both neutrons, a weight factor of 2 will be assigned to one neutron and the particular Maxwellian used for energy selection will be selected randomly assigning equal probability to both possibilities. This model, while not completely rigorous, is generally

felt to be more than adequate for fast reactor and critical assembly calculations. A more precise model could easily be incorporated into special purpose versions of VIM where n,2n reactions may play a more prominent role.

A logically simple, highly efficient method of generating the spatial source distribution has been developed. (Poor estimates of this source distribution can lead to incorrect values of k_{eff}, rendering an otherwise satisfactory Monte Carlo calculation useless.) The sensitivity of the estimate of k_{eff} to the spatial source distribution is likely to be higher in fast assemblies than thermal ones, making it imperative that the selection procedure adopted for use in VIM be completely reliable. Small, monoenergetic, bare spheres, however, have been shown to provide an even more severe test of a source selection procedure, since k_{eff} is governed entirely by leakage which is extremely sensitive to the source distribution in small systems. In addition, the criticality of monoenergetic bare spheres has been calculated analytically, and the results may be used as a standard against which the Monte Carlo procedures may be checked. A simple code was written to do this, and the anticipated variance difficulties were encountered. A procedure was ultimately developed which gave excellent results for even the smallest spheres tried without requiring us to resort to sophisticated sampling procedures. Treating the set of weighted source particle coordinates available at the start of a given generation as a distribution function from which individual particle coordinates may be selected, rather than by using the entire weighted set sequentially, proved to be the cure for all difficulties. The quality of our estimates of k_{eff} using this procedure compared favorably with more elaborate procedures found in the literature. (In fact, complicated estimation procedures were found to be necessary in all previously reported studies with which we are acquainted.) An important fringe benefit of the procedure we have adopted is the simplicity with which it can be incorporated into a large code such as VIM. This has now been done.

Interpretation of the adjoint techniques (developed during fiscal year 1968) in such a way that the transformation may be viewed as the introduction of an importance function obtainable analytically should permit the extension of a modified form of our technique to energy ranges where inelastic scattering may be important. This is exactly the approach which may be most useful in doing fixed source adjoint Monte Carlo calculation of reaction rates in small physical regions of fast reactors.

Work was completed on a topical report documenting the recently developed adjoint Monte Carlo techniques, including a full description of the STRIFE code, test problem results and interpretation, and a detailed exposition of the relation of this new work to the existing body of knowledge in this area. A more complete mapping of the effect on the variance of using adjoint Monte Carlo over the full range of resonance escape probabilities was found necessary to ensure adequate description of the effect in the topical report; consequently, some additional calculations were made of the resonance escape probability for a two-region repetitive slab lattice using the STRIFE code, the results of which are shown in the figure. The ratio of the variance obtained by using the untransformed (analog) adjoint technique to the variance obtained using the transformed adjoint technique is plotted against 1 - p. The advantage of the transformed adjoint technique over the analog adjoint technique is shown to be very large for small values of 1 - p. An interesting feature revealed by the more complete investigation is that the variance of the untransformed (analog) adjoint method appears to be always greater than that of the transformed method even for very high values of 1 - p where direct methods would normally have been thought to be more appropriate. In other words, the use of the transformed adjoint procedure always results in a variance reduction when compared with the untransformed procedure.

DOCUMENTATION – The following reports and papers were issued during the report period:

"Calculation of Reaction Rates in Small Physical Regions by Means of a New Non-Multigroup Adjoint Monte Carlo Technique," AI-AEC-12774 (March 15, 1969),

"A New Non-Multigroup Adjoint Monte Carlo Technique," Transactions of the ANS Topical Meeting on the Effective Use of Computer in the Nuclear Industry, April, 1969, and

"A New Non-Multigroup Adjoint Monte Carlo Technique," Nuclear Sci. and Eng., August, 1969.

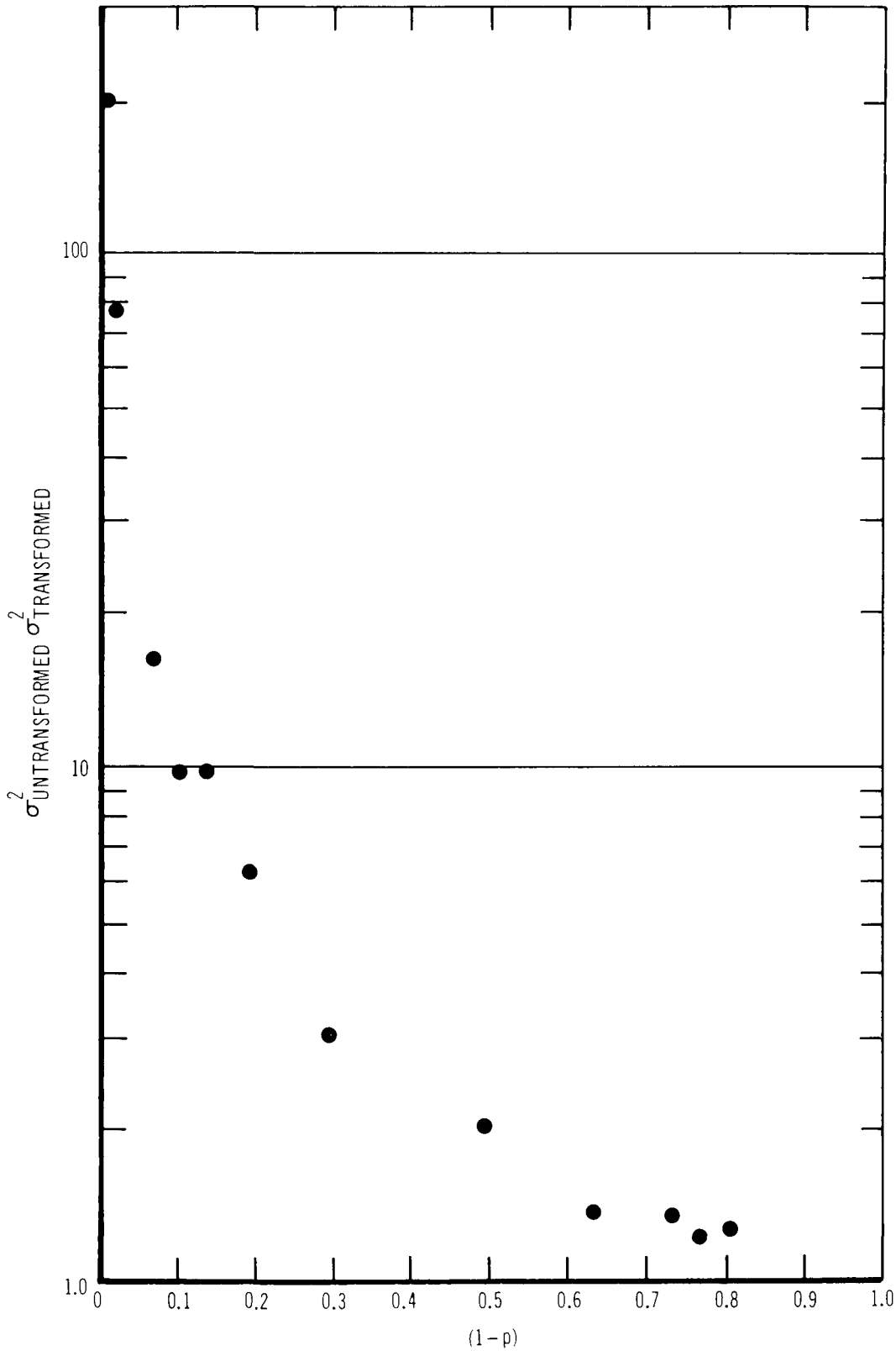

Computational Advantage of Adjoint Transformation

III. EVALUATION OF EFFORT

The major accomplishment of this fiscal year has been the completion of the first version of the VIM code. By far the most difficult and time consuming tasks have been the creation of a Monte Carlo cross-section library and the development of the complex bookkeeping procedures for storing this library in a high speed core. Virtually all of the procedures for doing this had to be developed at the time; or, in the case of existing procedures, drastic modification was necessary.

As a result, however, a major biproduct of the effort expended on this phase of the VIM program will be a suitable Monte Carlo library and data handling procedures which could be utilized generally for fast reactor Monte Carlo codes. Multigroup Monte Carlo methods have been avoided, since they severely compromise the purpose of the Monte Carlo method.

Insofar as was possible, basic cross-section data (σ versus E) and rigorous physical models have been adhered to. The inherent inefficiencies of a completely general geometry Monte Carlo code have been avoided and advantage has been taken of the essentially similar features of the major critical assemblies now in operation in developing the VIM geometry package.

Unnecessary particle splitting with its attendant complexities and risks has been avoided through the use of a simple but effective source generation procedure. The basic structure of the VIM code appears to be based on a sound plan, well suited to continual enlargement and modification as methods improve.

Program:	Reactor Physics
AEC Task:	26-A, Reactor Physics, Cross-Section Analysis
Project Manager:	H. A. Morewitz
Reporting Period:	Fiscal Year 1969
General Order: 7762	Subaccount: 13130 AEC Category: 04-40-01-03.1

Principal Scientists: H. Alter, G. L. Dunford

I. PROJECT OBJECTIVES

The objectives of this project include the evaluation, production, and maintenance of an up-to-date set of basic nuclear data; production and evaluation of multigroup constants; and the improvement of present day methods of neutronic calculations as related to microscopic and macroscopic nuclear data.

To accomplish these objectives, existing experimental and theoretical information on nuclear data will be surveyed, analyzed, and compiled. Automated methods will be utilized for manipulating and evaluating large amounts of available nuclear data and for the periodic updating of compiled data. Nuclear model calculations will be developed, extended, and used to help fill gaps in the data. The optical model analyses have two prime goals: to develop and test improved nuclear optical models for energy regions of interest to the fast reactor program and to develop sufficient confidence in the results of theoretical calculations so that they may be used confidently to predict neutron cross-section data where no experimental data are available. An automated system will be developed and maintained for the ready production of multigroup constants, and spectra generating techniques for production of realistic multigroup constants will be developed and incorporated into the system. The objectives of this project are related to Tasks 9-1.2, 9-1.3, 9-3.6 as outlined in the LMFBR Physics Program Plan, WASH-1109, Volume 9.

II. TECHNICAL PROGRESS DURING FISCAL YEAR 1969

A. COMPUTER GRAPHICS, SCORE, A MAN-COMPUTER INTERACTIVE NEUTRON CROSS-SECTION DATA EVALUATION SYSTEM

Significant progress in the development and utilization of the interactive computer graphics progress, SCORE, was made in several areas. Recoding

efforts associated with the present version of SCORE were completed. These included an overlay structure for SCORE which allows execution with a memory size of less than 180,000 bytes. The system was divided into five major independent segments to facilitate creation of the overlay structure. These segments are SCISRS data retrieval, SCISRS data manipulation, ENDF/B data retrieval and overlay, curve fitting, and resonance parameter analysis. In the process of recoding to create the overlay structure, many former coding inefficiencies were detected and eliminated. The presentation of information for many options was also improved. Care was taken to improve the ease with which the evaluator may use SCORE. With this objective in mind, routines were written to prevent termination of the execution of SCORE caused by input of unacceptable or incomplete data.

The graphics subroutines were modified to handle variable address IBM 2250 buffers such as the IBM 2250 Model III. In the process of this conversion, the program was modified to use 8K of buffer storage. If 8K is not available, 4K is used as an alternative. The extension to 8K buffer allows more data points to be displayed at one time; however, it has been noticed that some picture flutter is introduced when a large number of data points are plotted due to the increase in display generation time.

A cooperative effort, with Idaho Nuclear and Phillips Petroleum, whose goal is to produce an evaluator-usable, realistic, resonance-region, evaluation model, was begun. The new multilevel resonance module for SCORE was analyzed, programmed, and made operational. Extensive testing of this module was performed to detect and correct possible theory or programming errors. This program module was interfaced with SCORE and applied to the analysis and evaluation of MTR chopper data.

Verification was received that the cross-section evaluation group at Aldermaston (AWRE) have successfully executed SCORE II on an IBM 360 Model 40 which contains 128K bytes (32K words) of fast core memory. Because of this small memory size, however, they were forced to increase the number of program overlays and reduce their data storage capability. The Aldermaston group plans to make program modifications in order to produce hard copy via the Stromberg Carlson 4060. Upon checkout, these additions will be made available to other SCORE II users.

Documentation for SCORE II, AI-AEC-12757, was released for distribution, and the SCORE II computer code was deposited with the Argonne Code Center for general release.

Further improvements in SCORE II were made and will constitute SCORE III. All the graphics subroutines, which originally had been written in machine language, were converted into Fortran. The conversion, completed at Atomics International, was checked out in cooperation with IBM personnel at the Palo Alto IBM Scientific Center. Users of SCORE III will be able to easily modify current graphic subroutines as well as generate new ones.

Considerable effort was expended to upgrade the operating efficiency and the interactive capability of SCORE. The latest version of SCORE will operate within 110,000 bytes of fast memory with no sacrifice of the program's data display capacity. This reduction in required fast memory allows execution on computing systems whose normal mode of operation allocates 110,000 bytes of core to graphics and on machines with as little as 128,000 bytes of fast memory.

Many of the graphic display subroutines were modified to permit incremental update of graphic displays. These modifications permit more economical execution from a remote terminal such as is available at the MTR. Improvements were made in the interactive efficiency of many of the SCORE options.

To further utilization of the SCORE interactive computer system, a series of discussions were held with personnel at BNL, KAPL, and the University of Illinois at Urbana. At BNL, problems of interfacing the SCORE system computer graphics with the NNDC data information and retrieval system, SCISRS II, were discussed with D. Cullen; at KAPL, the principal topic dealt with how to best utilize the SCORE system on their computer hardware, which apparently is not fully compatible with SCORE software. At the University of Illinois, discussions were held with F. Adler on how to best utilize SCORE for the evaluation of fissile nuclide resonance data using the Adler-Adler multilevel resonance formalism.

B. ENDF/B DATA TESTING

1. Microscopic Cross-Sections

The Monte Carlo code TYCHE III was converted for, and was made operational on, the AI IBM 360/50 computer. This code, TYCHE IV, which was used as an aid in the Phase II data testing of the ENDF/B data files, calculates the first three infinite medium moments of the neutron slowing down density distribution. During the conversion process, several areas of the program were improved and the cross section library subroutine modified to read new library formats. A program, TYCHELIB, for generating a library for TYCHE IV, was completed and checked out. By use of this program, a library for hydrogen and oxygen (based on data used for the original age in water analysis) was generated and the neutron age in water calculated. The agreement between the presently calculated age and higher moments with earlier results computed on the IBM 7094 was satisfactory and is presented in Table 1.

TABLE 1

A COMPARISON OF TYCHE III AND IV CALCULATIONS FOR THE NEUTRON AGE AND HIGHER MOMENTS IN WATER

Code	$\tau^{\phi}(cm^2)$	$M_4^{\phi}(10^4 cm^4)$	$M_6^{\phi}(10^8 cm^6)$	$\langle E \rangle$ (Mev)	$\langle N \rangle$
TYCHE III	26.07 ± 0.09	9.55 ± 0.11	1.71 ± 0.05	1.985	15.7
TYCHE IV	26.09 ± 0.13	9.67 ± 0.13	1.72 ± 0.05	1.979	15.7
EXPERIMENT	26.46 ± 0.32	9.34 ± 0.50	1.37 ± 0.20	-	-

The TYCHE III results were based on a calculation using 80,000 neutron histories carried out in 1965. The TYCHE IV results were based on the current calculations for 40,000 neutron histories. $\langle E \rangle$ represents the calculated mean fission energy and $\langle N \rangle$, the mean number of collisions to indium resonance. The Cranberg fission spectrum defined by

$$f(E) = 0.453 \exp\left(\frac{-E}{0.965}\right) \sin h\ (2.29\ E)^{1/2}$$

was used for all calculations.

Another completed modification dealt with the method of treating differential elastic scattering data which is used to determine the degree of anisotropy in high energy neutron elastic collisions. Instead of generating and storing coefficients of a power series relating the cosine of the scattering angle, μ, to the cumulative probability distribution, ζ, the distribution, ζ, is stored at 21 equally spaced intervals in $\mu(\Delta\mu = 0.1)$ for each energy. Finally, a method allowing "naive" random number correlation was added to assure that each neutron history will start with the same random number, given identical initial random numbers. This allows one to determine more accurately the differences between the results for two cases with fewer histories.

A translator program, TYCHEB, was written to prepare ENDF/B cross section data for analysis and evaluation with TYCHE IV. The resulting punched card output consists of the energy and the total, elastic, and inelastic cross-sections for each isotope desired. The energy mesh for a given set of isotopes is obtained by merging the individual ENDF/B total cross-section energy grids for the isotopes in that set. The energy interval is from 1.0 ev to 10.0 Mev, and as many as three ENDF/B tapes may be used. The program was checked out and is operational on the S 360/50.

TYCHE IV cross-section libraries were prepared for hydrogen, deuterium, carbon, oxygen, aluminum, iron, and zirconium. Monte Carlo calculations of the neutron age to indium resonance were carried out in light water, heavy water, carbon, and in metal-water mixtures of aluminum, iron, and zirconium. All calculated results are based on sample sizes of 40,000 neutron histories and are believed to be adequately converged. Results of these calculations are presented in Table 2.

The ENDF/B cross sections for hydrogen, deuterium, carbon, and oxygen were compared with similar cross-section sets which were initially used to evaluate the neutron age measurements some years ago. The cross-sections compared quite well for hydrogen, reasonably well for oxygen, and poorly for deuterium and carbon. There was satisfactory agreement between the calculated and measured neutron age in light water; thus, one may conclude that the ENDF/B hydrogen and oxygen cross section evaluations are satisfactory. On the basis of the age calculation in heavy water and graphite, one concludes that the ENDF/B deuterium and carbon cross-sections are less than satisfactory.

TABLE 2

EVALUATION OF ENDF/B NUCLIDE CROSS-SECTIONS BY COMPARISON OF CALCULATED AND MEASURED NEUTRON AGE TO INDIUM RESONANCE
(40,000 neutron histories)

Moderator/Mixture	Atom Density (10^{22} atom/cm^3)		τ (cm^2)	
			Calculation	Experiment
H_2O	H:	6.688	26.09 ± 0.13	26.46 ± 0.32
	O:	3.344	-	-
D_2O (99.75%)	D:	6.60037	117.6 ± 0.2	111 ± 1
	H:	0.01672	-	109 ± 3
	O:	3.30855	-	-
Carbon	C:	8.0233	295.6 ± 0.5	307.8 ± 2.0
Al/H_2O (1.000)	Al:	3.0259	56.7 ± 0.2	59.6 ± 0.9
	H:	3.3370	-	-
	O:	1.6685	-	-
Fe/H_2O (1.737)	Fe:	5.3811	45.6 ± 0.1	46.4 ± 0.5
	H:	2.4372	-	-
	O:	1.2186	-	-
Zr/H_2O (1.200)	Zr:	2.3592	46.2 ± 0.2	49.7 ± 0.9
	H:	3.0282	-	-
	O:	1.5141	-	-

It was recommended that the ENDF/B deuterium and carbon scattering and total cross-sections be reevaluated.

It is more difficult to assess the validity of the ENDF/B metal nuclide cross-sections. For the homogeneous moderators, H_2O, D_2O and C, the experiments were relatively clean in the sense that there were no neutron streaming effects. In the metal water age measurements, the experimental systems were of heterogeneous arrangement and Palmedo* has demonstrated that anisotropic slowing down can be of significance in such systems. Homogeneous

*P. F. Palmedo, "Anisotropic Neutron Slowing Down in Aluminum - Water Mixtures," Parts I & II, NSE, 32 (302) June 1968

calculations for heterogeneous experimental systems generally tend to underestimate the measured age values. This is confirmed by the results given in Table 2. We conclude that the aluminum and zirconium cross sections are satisfactory, the iron data probably less so.

2. Data Evaluation By Correlation with Critical Assemblies

In the area of evaluation of the ENDF/B Phase II 'benchmark' calculations, the discrepancy between MC^2 results, for the ZPR-3-48 benchmark, of BNL and AI on the one hand vs those of ANL and LASL on the other, was partially resolved. The subroutine SIGVAC in the BNL and AI versions of MC^2 computes the smooth contribution to the resonance cross-section incorrectly when the smooth cross-section is negative. A correct version of this subroutine was obtained from R. LaBauve at LASL and the MC^2 calculation for ZPR-3-48 was repeated.

The incorporation of the correct version of the subroutine SIGVAC in MC^2 produced minor changes in the computed multigroup constants. The most significant change was a 15 to 20% decrease in the production term $\nu\Sigma_f$, between 300 and 1200 electron volts, an energy region which is of lesser importance in the analysis of the fast benchmark criticals. For example, the cross-section changes produced a change in k of 0.0031; i.e., from the original calculated value of 0.9862 to the present 0.9831.

In the ENDF/B Phase II data testing, a dual benchmark testing effort was completed. One route was the DAMMET-ETOE-MC^2 diffusion theory procedure (in use by ANL and LASL); the other involved the generation of data tapes in the AIENDF format from the ENDF/B tapes, then processing with the AI codes GRISM and AILMOE to produce multigroup sets for the diffusion code CAESAR. Results from CAESAR give k = 0.976 which is in reasonable agreement with results from ANL, k = 0.973 and LASL, k = 0.970. Both of the latter results were obtained by using DAMMET-ETOE-MC^2 as the processing mechanism. Tables 3 and 4 present results obtained for ZPR-3-48 and ZPR-3-11 in the dual benchmark testing effort.

TABLE 3

COMPARISON OF GRISM AND MC^2 RESULTS FOR k AND CENTRAL REACTION RATIOS IN ZPR-3-48 AND ZPR-3-11 USING ENDF/B DATA

Quantity	ZPR-3-48		ZPR-3-11	
	GRISM	MC^2	GRISM	MC^2
k	0.9758	0.9792	0.9792	0.9726
F_{24}/F_{25}	0.199	-	0.293	0.291
F_{26}/F_{25}	0.0697	-	0.0801	0.0784
F_{28}/F_{25}	0.0322	0.0338	0.0349	0.0343
F_{49}/F_{25}	0.928	0.940	-	-
F_{40}/F_{25}	0.234	0.244	-	-
C_{25}/F_{25}	-	0.269	0.194	0.192
C_{28}/F_{25}	0.145	0.137	0.117	0.117
C_{49}/F_{25}	0.194	0.186	-	-
A_{10_B}/F_{25}	1.295	-	-	-

TABLE 4

COMPARISON OF GRISM AND MC^2 RESULTS FOR CENTRAL REACTIVITY COEFFICIENTS IN ZPR-3-48 AND ZPR-3-11 USING ENDF/B DATA

Isotope	ZPR-3-48		ZPR-3-11	
	GRISM	MC^2	GRISM	MC^2
^{234}U	(2.89)	-	(11.76)	(11.89)
^{235}U	1.255	1.214	1.162	1.153
^{236}U	(-12.11)	-	(-4.04)	(-4.09)
^{238}U	1.33	1.19	1.25	1.30
^{239}Pu	1.236	1.219	-	-
^{240}Pu	1.03	1.16	-	-
^{241}Pu	(196.3)	(189.4)	-	-
Mo	2.26	2.12	-	-
Fe	1.42	1.37	1.24	1.15
Cr	2.27	1.34	1.21	0.43
Ni	1.23	0.97	1.37	0.94
Mn	3.12	1.89	1.56	1.34
Na	2.1	1.6	-	-
^{10}B	1.061	-	-	-
Al	1.28	1.33	-	-
C	4.6	3.0	-	-

The experimental values and the values which are enclosed in parentheses are in units of Ih/mole. The other entries are the ratio of calculated to experimental values.

3. GRISM and MC^2 Results Obtained by Using ENDF/B Data

Although the comparison of the results obtained with the libraries prepared by GRISM and MC^2 in Tables 3 and 4 shows generally good agreement, there are a few differences which are larger than expected. Since the same basic cross-section data are used in both calculations, better agreement between the values of k could be hoped for; furthermore, the central fission ratios from the calculation which uses the GRISM library for ZPR-3-48 are generally lower than the corresponding results from the calculation using the MC^2 library, while the ^{238}U and ^{239}Pu capture ratios are about 5% higher. The central reactivity coefficients for the ^{238}U and ^{240}Pu isotopes in ZPR-3-48 also show differences of about 10% in opposite directions. The spectra obtained with the MC^2 libraries are a little harder than the spectra with the GRISM libraries, as is shown in Table 5.

TABLE 5

MEDIAN FLUX ENERGY (kev) FOR ZPR-3-48 AND -11 WITH ENDF/B CROSS SECTIONS

Location	ZPR-3-48		ZPR-3-11	
	GRISM	MC^2	GRISM	MC^2
Core center	198.1	211.3	305.8	310.0
Core average	183.3	194.6	291.4	295.8
Blanket	139.7	139.9	170.1	174.7

One likely source of the preceding differences appears to be the group cross sections computed in the resonance energy region. The MC^2 calculation takes resonance overlap into account, and forms the multigroup cross sections by collapsing the fine-group cross sections. On the other hand, the GRISM calculation assumes isolated resonances and forms the multigroup cross section by weighting the effective resonance integrals of each resolved resonance and of a number of energy points for the unresolved resonances, with the AILMOE ultrafine-group spectrum. The multigroup absorption cross sections for ^{238}U and ^{239}Pu, and the multigroup transport cross sections for ^{238}U and Fe in ZPR-3-48 are compared in Table 6.

TABLE 6

MULTIGROUP CROSS SECTIONS FOR ^{238}U, ^{239}Pu, AND Fe IN ZPR-3-48

Group	E_{MIN} (kev)	$\sigma_a(28)$		$\sigma_a(49)$		$\sigma_{tr}(28)$		$\sigma_{tr}(Fe)$	
		GRISM	MC^2	GRISM	MC^2	GRISM	MC^2	GRISM	MC^2
1	6,065.	0.329	0.266	2.07	2.09	3.67	3.63	1.84	1.81
2	3,679.	0.583	0.584	1.90	1.90	4.23	4.20	2.22	2.19
3	2,231.	0.488	0.587	2.01	2.01	4.64	4.63	2.33	2.31
4	1,353.	0.487	0.493	1.93	1.93	5.02	5.02	2.35	2.33
5	821.	0.173	0.172	1.80	1.80	4.93	4.93	1.98	1.95
6	498.	0.141	0.141	1.71	1.71	5.80	5.77	2.34	2.31
7	302.0	0.135	0.135	1.64	1.64	7.13	7.09	3.01	2.97
8	183.2	0.151	0.151	1.66	1.66	8.58	8.55	2.90	2.53
9	111.1	0.181	0.181	1.72	1.73	9.97	9.98	4.66	3.31
10	67.4	0.236	0.235	1.73	1.73	11.34	11.32	4.86	3.61
11	40.9	0.334	0.332	1.78	1.77	11.50	12.33	4.30	4.05
12	24.8	0.458	0.438	2.14	2.11	10.81	13.18	8.82	4.97
13	15.03	0.546	0.557	2.57	2.55	11.02	14.32	1.76	1.27
14	9.12	0.670	0.673	3.06	3.04	11.22	14.85	5.21	4.80
15	5.53	0.782	0.782	3.68	3.61	11.35	14.85	12.00	10.48
16	3.35	0.953	0.860	4.30	4.26	12.23	9.61	5.43	5.09
17	2.03	1.330	1.104	5.71	5.70	21.38	14.04	6.06	5.61
18	1.234	1.256	0.927	6.96	7.02	19.59	13.72	7.40	6.92
19	0.749	1.436	1.105	8.75	8.83	22.41	5.00	9.12	8.59
20	0.454	1.262	0.984	12.80	12.75	17.48	10.51	10.07	9.49
21	0.275	1.127	0.986	13.07	12.62	16.81	10.66	10.73	10.14
22	0.167	1.718	1.213	23.08	21.52	45.62	7.36	11.17	10.59
23	0.101	2.431	1.544	29.96	24.82	48.31	10.67	11.29	10.71
24	0.061	1.944	1.817	32.96	23.74	46.58	1.94	11.31	10.75
25	0.037	0.782	0.429	64.78	63.58	67.39	11.30	11.28	10.73
26	0.023	5.405	3.683	13.20	13.87	134.63	9.12	11.28	10.75

ENDF/B resolved resonance data extends to 3904 ev for ^{238}U and to 298 ev for ^{239}Pu. Table 6 shows that the agreement of the absorption cross sections is good, except in the resolved resonance region, where MC^2 and GRISM results differ. Qualitatively, these differences are due to the different methods of treating the resolved resonances by the two codes.

The multigroup transport cross sections for ^{238}U and Fe are also compared in Table 6. In ^{238}U, the agreement is good above 67 kev, but significant differences appear below this energy. The MC^2 results are generally larger at higher energies than the GRISM results; but, below 3.3 kev, the reverse is true. Some of the differences at low energy are quite large and are due to the fact the GRISM weighting spectrum does not contain the flux dips caused by the resonances in the fuel isotopes.

The agreement in Fe is good above 302 kev; while, below this energy, the MC^2 results are lower than the GRISM results. In comparison, the GRISM and MC^2 transport cross-sections for carbon generally agree, to better than 1%.

Since less than 4% of the central flux in ZPR-3-48 is below 3.3 kev, the GRISM and MC^2 cross-section differences for ^{238}U cannot introduce a very large difference in the value of C_{28}/F_{25} and the central reactivity worth of ^{238}U in this assembly.

The MC**2 macroscopic group constants for ZPR-3-48 core and blanket, and for ZPR-3-11 core and blanket, were received from ANL, BNL, and LASL for processing and evaluation. The processing of all data was completed.

All installations used the fine group mode in MC**2 to generate the multigroup constants. In addition, Los Alamos generated the data in the ultra fine (UF) mode. Results obtained thus far illustrate variations in multigroup constants and fluxes. These variations, along with, in some cases, significant differences in the values of the multigroup constants, are difficult to understand. Since calculation of these 'constants' proceeded from both the same data base and with the same processing codes, the reasons for these variations are not fully understood and may prove detrimental to present and future CSEWG Phase II data testing. Logically, one would expect the variation in the multigroup values to be minimal. This is not the case.

For ZPR-3-48, the core multigroup constants are compared in Tables 7 through 14. The core flux and adjoint are compared in Tables 15 and 16.

TABLE 7

MC**2 26 GROUP MACROSCOPIC TRANSPORT CROSS SECTIONS (ZPR-3-48 CORE)
CSEWG PHASE 2 ENDF/B DATA TESTING

ENERGY (EV)	AI	ANL	BNL	LASL	LASL (UF)
6.0653E 06	8.7060E-02	8.8912E-02	8.7046E-02	8.6746E-02	8.8607E-02
3.6788E 06	1.0430E-01	1.0618E-01	1.0428E-01	1.0395E-01	1.0584E-01
2.2313E 06	1.2222E-01	1.2256E-01	1.2221E-01	1.2181E-01	1.2215E-01
1.3534E 06	1.2743E-01	1.2824E-01	1.2740E-01	1.2695E-01	1.2778E-01
8.2085E 05	1.3837E-01	1.3921E-01	1.3835E-01	1.3786E-01	1.3870E-01
4.9787E 05	1.6940E-01	1.7115E-01	1.6938E-01	1.6874E-01	1.7049E-01
3.0197E 05	1.9636E-01	1.9855E-01	1.9634E-01	1.9537E-01	1.9756E-01
1.8316E 05	2.1689E-01	2.2161E-01	2.1686E-01	2.1552E-01	2.2021E-01
1.1109E 05	2.4582E-01	2.5789E-01	2.4579E-01	2.4487E-01	2.5683E-01
6.7380E 04	2.6377E-01	2.7896E-01	2.6384E-01	2.6264E-01	2.7746E-01
4.0868E 04	2.8539E-01	2.9809E-01	2.8542E-01	2.8523E-01	2.9785E-01
2.4788E 04	3.0712E-01	3.4697E-01	3.0776E-01	3.0647E-01	3.4564E-01
1.5034E 04	3.0355E-01	3.1383E-01	3.0360E-01	3.0319E-01	3.1342E-01
9.1188E 03	3.5748E-01	3.6607E-01	3.5743E-01	3.5720E-01	3.6582E-01
5.5308E 03	4.3344E-01	4.5198E-01	4.3428E-01	4.3308E-01	4.5058E-01
3.3546E 03	4.2757E-01	4.7375E-01	4.5699E-01	4.2712E-01	4.4399E-01
2.0347E 03	5.8259E-01	5.8186E-01	5.9414E-01	5.8205E-01	5.6876E-01
1.2341E 03	2.8859E-01	3.2501E-01	3.1685E-01	2.8817E-01	2.9619E-01
7.4852E 02	3.1016E-01	3.5648E-01	3.5025E-01	3.0964E-01	3.1737E-01
4.5400E 02	3.6314E-01	3.7321E-01	3.6937E-01	3.6277E-01	3.7151E-01
2.7536E 02	3.8498E-01	4.0038E-01	3.9630E-01	3.8482E-01	3.9184E-01
1.6702E 02	3.5050E-01	3.6539E-01	3.6490E-01	3.5050E-01	3.5351E-01
1.0130E 02	3.9636E-01	3.9590E-01	3.9831E-01	3.9583E-01	3.9300E-01
6.1442E 01	3.3079E-01	3.2834E-01	3.3701E-01	3.3668E-01	3.2774E-01
3.7266E 01	4.6059E-01	4.4285E-01	4.6193E-01	4.6199E-01	4.4224E-01
2.2603E 01	3.6795E-01	3.6191E-01	3.6911E-01	3.6929E-01	3.6167E-01

TABLE 8

MC**2 26 GROUP MACROSCOPIC FISSION CROSS SECTIONS (ZPR-3-48 CORE)
CSEWG PHASE 2 ENDF/B DATA TESTING

ENERGY (EV)	AI	ANL	BNL	LASL	LASL (UF)
6.0653E 06	1.0763E-02	1.0748E-02	1.0756E-02	1.0757E-02	1.0748E-02
3.6788E 06	7.5597E-03	7.5531E-03	7.5535E-03	7.5533E-03	7.5531E-03
2.2313E 06	7.6539E-03	7.6476E-03	7.6483E-03	7.6481E-03	7.6476E-03
1.3534E 06	6.4791E-03	6.4810E-03	6.4735E-03	6.4735E-03	6.4812E-03
8.2085E 05	3.2749E-03	3.2721E-03	3.2700E-03	3.2699E-03	3.2722E-03
4.9787E 05	2.7961E-03	2.7937E-03	2.7942E-03	2.7942E-03	2.7937E-03
3.0197E 05	2.5325E-03	2.5315E-03	2.5318E-03	2.5320E-03	2.5315E-03
1.8316E 05	2.4899E-03	2.4897E-03	2.4897E-03	2.4897E-03	2.4897E-03
1.1109E 05	2.5499E-03	2.5504E-03	2.5498E-03	2.5498E-03	2.5504E-03
6.7380E 04	2.5531E-03	2.5519E-03	2.5528E-03	2.5528E-03	2.5519E-03
4.0868E 04	2.4969E-03	2.4973E-03	2.4965E-03	2.4965E-03	2.4973E-03
2.4788E 04	2.7393E-03	2.7484E-03	2.7389E-03	2.7387E-03	2.7481E-03
1.5034E 04	3.1025E-03	3.1034E-03	3.1023E-03	3.1023E-03	3.1034E-03
9.1188E 03	3.5394E-03	3.5394E-03	3.5399E-03	3.5401E-03	3.5394E-03
5.5308E 03	4.0823E-03	4.0907E-03	4.0850E-03	4.0861E-03	4.0913E-03
3.3546E 03	4.6868E-03	4.6961E-03	4.6935E-03	4.6960E-03	4.6977E-03
2.0347E 03	6.0655E-03	6.0787E-03	6.0579E-03	6.0617E-03	6.0810E-03
1.2341E 03	7.3710E-03	7.3581E-03	7.3532E-03	7.3630E-03	7.3613E-03
7.4852E 02	9.2049E-03	9.2069E-03	1.0351E-02	9.2083E-03	9.2073E-03
4.5400E 02	1.3178E-02	1.3323E-02	1.6028E-02	1.3199E-02	1.3319E-02
2.7536E 02	1.3443E-02	1.3298E-02	1.6827E-02	1.3559E-02	1.3294E-02
1.6702E 02	2.5059E-02	2.6289E-02	2.5266E-02	2.5341E-02	2.6286E-02
1.0130E 02	2.6237E-02	2.6608E-02	2.6517E-02	2.6618E-02	2.6601E-02
6.1442E 01	3.4692E-02	3.8465E-02	3.8702E-02	3.8817E-02	3.8454E-02
3.7266E 01	7.1431E-02	8.2122E-02	7.2291E-02	7.2681E-02	8.2124E-02
2.2603E 01	1.3124E-02	1.4202E-02	1.3299E-02	1.3363E-02	1.4197E-02

TABLE 9

MC**2 26 GROUP MACROSCOPIC CAPTURE CROSS SECTIONS (ZPR-3-48 CORE)
CSEWG PHASE 2 ENDF/B DATA TESTING

ENERGY (EV)	AI	ANL	BNL	LASL	LASL (UF)
6.0653E 06	2.0075E-03	1.9939E-03	2.0074E-03	1.9765E-03	1.9627E-03
3.6788E 06	5.3877E-04	5.3790E-04	5.3851E-04	5.3587E-04	5.3508E-04
2.2313E 06	3.8622E-04	3.8608E-04	3.8615E-04	3.8546E-04	3.8542E-04
1.3534E 06	6.2943E-04	6.2029E-04	6.2147E-04	6.2846E-04	6.2729E-04
8.2085E 05	1.2291E-03	1.2281E-03	1.2290E-03	1.2276E-03	1.2267E-03
4.9787E 05	1.2842E-03	1.2838E-03	1.2839E-03	1.2825E-03	1.2825E-03
3.0197E 05	1.3303E-03	1.3307E-03	1.3300E-03	1.3285E-03	1.3293E-03
1.8316E 05	1.5340E-03	1.5346E-03	1.5337E-03	1.5324E-03	1.5334E-03
1.1109E 05	1.8182E-03	1.8209E-03	1.8179E-03	1.8162E-03	1.8194E-03
6.7380E 04	2.2472E-03	2.2502E-03	2.2467E-03	2.2451E-03	2.2496E-03
4.0868E 04	3.1151E-03	3.1230E-03	3.1150E-03	3.1129E-03	3.1208E-03
2.4788E 04	4.4672E-03	4.5276E-03	4.2903E-03	4.4666E-03	4.5229E-03
1.5034E 04	5.7229E-03	5.7360E-03	5.7303E-03	5.7319E-03	5.7351E-03
9.1188E 03	7.0989E-03	7.1182E-03	7.0994E-03	7.1196E-03	7.1172E-03
5.5308E 03	9.0923E-03	9.1458E-03	9.1221E-03	9.1316E-03	9.1445E-03
3.3546E 03	9.9381E-03	9.9864E-03	9.9520E-03	9.9402E-03	9.9854E-03
2.0347E 03	1.3299E-02	1.3411E-02	1.3267E-02	1.3284E-02	1.3411E-02
1.2341E 03	1.2706E-02	1.2791E-02	1.2785E-02	1.2826E-02	1.2790E-02
7.4852E 02	1.7166E-02	1.7504E-02	1.7332E-02	1.7387E-02	1.7500E-02
4.5400E 02	1.7318E-02	1.7666E-02	1.9011E-02	1.7619E-02	1.7656E-02
2.7536E 02	1.8651E-02	1.8964E-02	1.8870E-02	1.9036E-02	1.8854E-02
1.6702E 02	2.2053E-02	2.3670E-02	2.2498E-02	2.2656E-02	2.3658E-02
1.0130E 02	3.2395E-02	3.2988E-02	3.2986E-02	3.3208E-02	3.2968E-02
6.1442E 01	2.3044E-02	2.4363E-02	2.5336E-02	2.5501E-02	2.4344E-02
3.7266E 01	4.4643E-02	4.6148E-02	4.5080E-02	4.5359E-02	4.6118E-02
2.2603E 01	4.1129E-02	5.1977E-02	4.2268E-02	4.2639E-02	5.1954E-02

TABLE 10

MC**2 26 GROUP MACROSCOPIC INELASTIC CROSS SECTIONS (ZPR-3-48 CORE)
CSEWG PHASE 2 ENDF/B DATA TESTING

ENERGY (EV)	AI	ANL	BNL	LASL	LASL (UF)
6.0653E 06	4.3246E-02	4.3283E-02	4.3241E-02	4.3062E-02	4.3103E-02
3.6788E 06	4.6962E-02	4.6951E-02	4.6956E-02	4.6787E-02	4.6781E-02
2.2313E 06	4.0002E-02	4.0002E-02	3.9996E-02	3.9895E-02	3.9900E-02
1.3534E 06	3.6115E-02	3.6117E-02	3.6108E-02	3.6066E-02	3.6074E-02
8.2085E 05	2.5513E-02	2.5549E-02	2.5506E-02	2.5492E-02	2.5538E-02
4.9787E 05	1.6624E-02	1.6612E-02	1.6619E-02	1.6619E-02	1.6612E-02
3.0197E 05	1.2096E-02	1.2068E-02	1.2092E-02	1.2092E-02	1.2068E-02
1.8316E 05	9.4589E-03	9.4475E-03	9.4551E-03	9.4561E-03	9.4487E-03
1.1109E 05	7.0637E-03	7.0321E-03	7.0615E-03	7.0616E-03	7.0328E-03
6.7380E 04	3.5997E-03	3.5787E-03	3.5984E-03	3.5974E-03	3.5789E-03
4.0868E 04	1.0373E-03	1.0222E-03	1.0363E-03	1.0368E-03	1.0229E-03
2.4788E 04	3.7515E-04	3.7410E-04	3.7510E-04	3.7517E-04	3.7423E-04
1.5034E 04	3.3597E-04	3.3574E-04	3.3593E-04	3.3598E-04	3.3582E-04
9.1188E 03	2.1974E-04	2.2000E-04	2.1977E-04	2.1975E-04	2.2001E-04
5.5308E 03	1.4386E-05	1.3925E-05	1.4395E-05	1.4384E-05	1.3916E-05

TABLE 11

MC**2 26 GROUP MACROSCOPIC N,2N CROSS SECTIONS (ZPR-3-48 CORE)
CSEWG PHASE 2 ENDF/B DATA TESTING

ENERGY (EV)	AI	ANL	BNL	LASL	LASL (UF)
6.0653E 06	5.1959E-03	5.1594E-03	5.1954E-03	5.1959E-03	5.1598E-03
3.6788E 06	1.5066E-06	1.4869E-06	1.5048E-06	1.5086E-06	1.4903E-06

TABLE 12

MC**2 26 GROUP MACROSCOPIC INELASTIC TRANSFER ELEMENTS (ZPR-3-48 CORE)
CSEWG PHASE 2 ENDF/B DATA TESTING

GROUP 1 TO	AI	ANL	BNL	LASL	LASL (UF)
1	4.6952E-04	4.6582E-04	4.6738E-04	4.5350E-04	4.5190E-04
2	3.6585E-03	3.6496E-03	3.6789E-03	3.6360E-03	3.6060E-03
3	8.0727E-03	8.2708E-03	8.2683E-03	8.2210E-03	8.2230E-03
4	9.9535E-03	1.0657E-02	1.0633E-02	1.0600E-02	1.0620E-02
5	8.1983E-03	9.2943E-03	9.2957E-03	9.2750E-03	9.2730E-03
6	6.4081E-03	7.4280E-03	7.4433E-03	7.4340E-03	7.4180E-03
7	4.6126E-03	5.2841E-03	5.2979E-03	5.2940E-03	5.2800E-03
8	3.3268E-03	3.6849E-03	3.6888E-03	3.6870E-03	3.6840E-03
9	2.2207E-03	2.3889E-03	2.3868E-03	2.3860E-03	2.3890E-03
10	1.2693E-03	1.3422E-03	1.3392E-03	1.3390E-03	1.3420E-03
11	6.2698E-04	6.5688E-04	6.5489E-04	6.5480E-04	6.5700E-04
12	2.7834E-04	2.9014E-04	2.8913E-04	2.8910E-04	2.9020E-04
13	1.1460E-04	1.1914E-04	1.1869E-04	1.1870E-04	1.1920E-04
14	4.3986E-05	4.5702E-05	4.5518E-05	4.5520E-05	4.5720E-05
15	1.5781E-05	1.6145E-05	1.6077E-05	1.6080E-05	1.6150E-05
16	5.7387E-06	5.7685E-06	5.7377E-06	5.7370E-06	5.7710E-06
17	2.0056E-06	2.0202E-06	2.0052E-06	2.0050E-06	2.0210E-06
18	4.6276E-07	4.6554E-07	4.6270E-07	4.6270E-07	4.6630E-07

TABLE 13

MC**2 MACROSCOPIC ELASTIC TRANSFER ELEMENTS (ZPR-3-48 CORE)
CSEWG PHASE 2 ENDF/B DATA TESTING

INTO GROUP	AI	ANL	BNL	LASL	LASL (UF)
1	1.8110E-02	1.7843E-02	1.7772E-02	1.8040E-02	1.7770E-02
2	3.5975E-02	3.5529E-02	3.5968E-02	3.5850E-02	3.5400E-02
3	5.9396E-02	5.6923E-02	5.9404E-02	5.9160E-02	5.6860E-02
4	6.8928E-02	6.7230E-02	6.8909E-02	6.8560E-02	6.6870E-02
5	8.7517E-02	8.4975E-02	8.7491E-02	8.7100E-02	8.4590E-02
6	1.2252E-01	1.2061E-01	1.2249E-01	1.2200E-01	1.2000E-01
7	1.5197E-01	1.5041E-01	1.5196E-01	1.5110E-01	1.4960E-01
8	1.7279E-01	1.7359E-01	1.7277E-01	1.7160E-01	1.7240E-01
9	2.0168E-01	2.0949E-01	2.0166E-01	2.0090E-01	2.0860E-01
10	2.2064E-01	2.3171E-01	2.2072E-01	2.1990E-01	2.3060E-01
11	2.4188E-01	2.5023E-01	2.4192E-01	2.4180E-01	2.5010E-01
12	2.5805E-01	2.9557E-01	2.5885E-01	2.5760E-01	2.9440E-01
13	2.5890E-01	2.6278E-01	2.5895E-01	2.5860E-01	2.6250E-01
14	3.0876E-01	3.1271E-01	3.0872E-01	3.0850E-01	3.1250E-01
15	3.7635E-01	3.8865E-01	3.7717E-01	3.7610E-01	3.8740E-01
16	3.5935E-01	3.9775E-01	3.8868E-01	3.5890E-01	3.6810E-01
17	4.3883E-01	4.4768E-01	4.5044E-01	4.3840E-01	4.3470E-01
18	2.2955E-01	2.6222E-01	2.5766E-01	2.2910E-01	2.3360E-01
19	2.4783E-01	2.8975E-01	2.8713E-01	2.4720E-01	2.5070E-01
20	3.0032E-01	3.0634E-01	3.0206E-01	2.9980E-01	3.0470E-01
21	3.1603E-01	3.2821E-01	3.2401E-01	3.1550E-01	3.1980E-01
22	2.6736E-01	2.7869E-01	2.8120E-01	2.6670E-01	2.6390E-01
23	3.0414E-01	3.0273E-01	3.0538E-01	3.0270E-01	2.9990E-01
24	2.4165E-01	2.3563E-01	2.4412E-01	2.4360E-01	2.3510E-01
25	3.1677E-01	2.8339E-01	3.1700E-01	3.1650E-01	2.8290E-01
26	2.7339E-01	2.5037E-01	2.7339E-01	2.7330E-01	2.5020E-01

TABLE 14

MC**2 MACROSCOPIC ELASTIC TRANSFER ELEMENTS (ZPR-3-48 CORE)
CSEWG PHASE 2 ENDF/B DATA TESTING

OUT OF GROUP	AI	ANL	BNL	LASL	LASL (UF)
1	7.7365E-03	9.8844E-03	7.7350E-03	7.7160E-03	9.8590E-03
2	1.3265E-02	1.5604E-02	1.3258E-02	1.3220E-02	1.5560E-02
3	1.4786E-02	1.7605E-02	1.4771E-02	1.4710E-02	1.7540E-02
4	1.5276E-02	1.7795E-02	1.5289E-02	1.5220E-02	1.7720E-02
5	2.0834E-02	2.4184E-02	2.0850E-02	2.0770E-02	2.4070E-02
6	2.6175E-02	2.9857E-02	2.6181E-02	2.6090E-02	2.9670E-02
7	2.8429E-02	3.2217E-02	2.8431E-02	2.8280E-02	3.2060E-02
8	3.0618E-02	3.4545E-02	3.0617E-02	3.0430E-02	3.4350E-02
9	3.2707E-02	3.6997E-02	3.2705E-02	3.2560E-02	3.6840E-02
10	3.4733E-02	3.8870E-02	3.4730E-02	3.4360E-02	3.8500E-02
11	3.6864E-02	4.1214E-02	3.6859E-02	3.6780E-02	4.1100E-02
12	4.1496E-02	4.3759E-02	4.1506E-02	4.1300E-02	4.3560E-02
13	3.5491E-02	4.1876E-02	3.5482E-02	3.5390E-02	4.1780E-02
14	3.7867E-02	4.2482E-02	3.7855E-02	3.7790E-02	4.2410E-02
15	4.3902E-02	5.0075E-02	4.3885E-02	4.3790E-02	4.9960E-02
16	5.3596E-02	6.1313E-02	5.3662E-02	5.3540E-02	6.1180E-02
17	1.2439E-01	1.1470E-01	1.2438E-01	1.2430E-01	1.1460E-02
18	3.8962E-02	4.2647E-02	3.9046E-02	3.8960E-02	4.2450E-02
19	3.5964E-02	4.0016E-02	3.5440E-02	3.5830E-02	3.9920E-02
20	3.2316E-02	3.5884E-02	3.2274E-02	3.2180E-02	3.5810E-02
21	3.6855E-02	4.0012E-02	3.6592E-02	3.6690E-02	3.9920E-02
22	3.6021E-02	3.9742E-02	3.5934E-02	3.5810E-02	3.9640E-02
23	3.3589E-02	3.3575E-02	3.3425E-02	3.3300E-02	3.3500E-02
24	3.1405E-02	2.9889E-02	2.8847E-02	2.8720E-02	2.9820E-02
25	2.7749E-02	3.1188E-02	2.7572E-02	2.7460E-02	3.1120E-02

TABLE 15

COMPARISON OF MC**2 26 GROUP FLUXES (ZPR-3-48 CORE)
CSEWG PHASE 2 ENDF/B DATA TESTING

ENERGY (EV)	AI	ANL	BNL	LASL	LASL (UF)
6.0653E 06	4.2031E-01	4.0691E-01	4.1737E-01	4.1916E-01	4.0813E-01
3.6788E 06	1.7050E 00	1.6545E 00	1.6946E 00	1.7010E 00	1.6588E 00
2.2313E 06	3.7292E 00	3.6027E 00	3.7119E 00	3.7248E 00	3.6108E 00
1.3534E 06	5.3945E 00	5.2854E 00	5.3871E 00	5.4044E 00	5.2946E 00
8.2085E 05	7.2177E 00	6.9657E 00	7.2474E 00	7.2740E 00	6.9757E 00
4.9787E 05	9.8972E 00	9.4324E 00	9.9582E 00	1.0002E 01	9.4470E 00
3.0197E 05	1.1664E 01	1.1071E 01	1.1725E 01	1.1796E 01	1.1103E 01
1.8316E 05	1.1263E 01	1.0757E 01	1.1298E 01	1.1374E 01	1.0790E 01
1.1109E 05	9.9756E 00	9.5832E 00	9.9811E 00	1.0033E 01	9.5980E 00
6.7380E 04	8.6135E 00	8.4382E 00	8.5934E 00	8.6814E 00	8.4820E 00
4.0868E 04	7.2129E 00	7.1355E 00	7.1743E 00	7.1961E 00	7.1284E 00
2.4788E 04	5.4608E 00	5.7599E 00	5.4348E 00	5.4479E 00	5.7622E 00
1.5034E 04	4.9481E 00	4.8244E 00	4.9094E 00	4.9109E 00	4.8140E 00
9.1188E 03	3.5152E 00	3.6895E 00	3.4779E 00	3.4769E 00	3.6793E 00
5.5308E 03	2.2869E 00	2.4292E 00	2.2567E 00	2.2570E 00	2.4229E 00
3.3546E 03	1.4436E 00	1.5738E 00	1.4220E 00	1.4205E 00	1.5665E 00
2.0347E 03	5.3538E-01	7.1387E-01	5.2790E-01	5.2653E-01	7.0951E-01
1.2341E 03	1.0815E 00	1.2554E 00	1.0651E 00	1.0603E 00	1.2458E 00
7.4852E 02	6.5092E-01	7.7635E-01	6.3610E-01	6.3447E-01	7.6500E-01
4.5400E 02	3.6086E-01	4.5004E-01	3.2449E-01	3.4894E-01	4.4302E-01
2.7536E 02	1.6448E-01	2.1767E-01	1.4094E-01	1.5744E-01	2.1404E-01
1.6702E 02	7.1084E-02	9.4773E-02	6.0048E-02	6.7125E-02	9.2997E-02
1.0130E 02	2.7207E-02	3.9558E-02	2.2728E-02	2.5278E-02	3.8762E-02
6.1442E 01	9.9975E-03	1.3954E-02	7.9740E-03	8.8258E-03	1.3659E-02
3.7266E 01	2.1596E-03	2.5870E-03	1.5687E-03	1.7231E-03	2.5280E-03
2.2603E 01	6.2099E-04	7.0973E-04	4.4223E-04	4.8260E-04	6.9269E-04

TABLE 16

COMPARISON OF MC**2 26 GROUP ADJOINT FLUXES (ZPR-3-48 CORE)
CSEWG PHASE 2 ENDF/B DATA TESTING

ENERGY (EV)	AI	ANL	BNL	LASL	LASL (UF)
6.0653E 06	1.2277E 00	1.2691E 00	1.2717E 00	1.2743E 00	1.2704E 00
3.6788E 06	1.0555E 00	1.0999E 00	1.0992E 00	1.1007E 00	1.1003E 00
2.2313E 06	1.0703E 00	1.0836E 00	1.0868E 00	1.0880E 00	1.0840E 00
1.3534E 06	1.0252E 00	1.0050E 00	1.0066E 00	1.0071E 00	1.0050E 00
8.2085E 05	9.2611E-01	9.0986E-01	9.0787E-01	9.0806E-01	9.0975E-01
4.9787E 05	9.1997E-01	9.0588E-01	9.0344E-01	9.0295E-01	9.0562E-01
3.0197E 05	9.1054E-01	9.0054E-01	8.9732E-01	8.9518E-01	9.0003E-01
1.8316E 05	9.0080E-01	8.9534E-01	8.9116E-01	8.8719E-01	8.9465E-01
1.1109E 05	8.8921E-01	8.8774E-01	8.8314E-01	8.7727E-01	8.8695E-01
6.7380E 04	8.7016E-01	8.7182E-01	8.6753E-01	8.5939E-01	8.7072E-01
4.0868E 04	8.5326E-01	8.5764E-01	8.5413E-01	8.4340E-01	8.5621E-01
2.4788E 04	8.5023E-01	8.5731E-01	8.5506E-01	8.4096E-01	8.5531E-01
1.5034E 04	8.5950E-01	8.6586E-01	8.6494E-01	8.5055E-01	8.6333E-01
9.1188E 03	8.8339E-01	8.8989E-01	8.9457E-01	8.7472E-01	8.9650E-01
5.5308E 03	9.1316E-01	9.2082E-01	9.3121E-01	9.0439E-01	9.1623E-01
3.3546E 03	9.5740E-01	9.6340E-01	9.8439E-01	9.4808E-01	9.5742E-01
2.0347E 03	1.0001E 00	1.0018E 00	1.0351E 00	9.8917E-01	9.9594E-01
1.2341E 03	1.0266E 00	1.0325E 00	1.0678E 00	1.0144E 00	1.0258E 00
7.4852E 02	1.0836E 00	1.0872E 00	1.1493E 00	1.0711E 00	1.0825E 00
4.5400E 02	1.2194E 00	1.2162E 00	1.2856E 00	1.2072E 00	1.2156E 00
2.7536E 02	1.2816E 00	1.2774E 00	1.3461E 00	1.2713E 00	1.2762E 00
1.6702E 02	1.4218E 00	1.4174E 00	1.4168E 00	1.4140E 00	1.4164E 00
1.0130E 02	1.3744E 00	1.3831E 00	1.3735E 00	1.3718E 00	1.3832E 00
6.1442E 01	1.6141E 00	1.6523E 00	1.6292E 00	1.6290E 00	1.6530E 00
3.7266E 01	1.5334E 00	1.5735E 00	1.5352E 00	1.5366E 00	1.5744E 00
2.2603E 01	6.6346E-01	5.9125E-01	6.5504E-01	6.5428E-01	5.9136E-01

4. Optical Model Analysis and Development

Two new nuclear reaction theory codes were completed. The first code is a deformed nucleus scattering code which couples together the ground state and the first two excited levels (0+, 2+, 4+). The deformed potential has been expanded and terms up to second order in the deformation have been retained (previously only first order terms were retained). A new feature is the ability to calculate Legendre moments of the scattering angular distributions directly from the scattering matrix.

The second code is a compound nucleus reaction theory code. This program uses a statistical theory to separate the compound nucleus or "absorption" cross section into its component parts. Fluctuation corrections can be applied to the partial cross sections and to the Legendre coefficients of elastic and inelastic neutron angular distributions. A continuum model for inelastic neutron emission and the n,2n reaction have been included. Both a discrete level and a continuum neutron fission model are available. Penetrabilities for various neutron energies can be calculated internally using a spherical optical model or may be supplied by card input. The models, contained in these codes, are to be used for an analysis of uranium-238 cross sections above several kilovolts.

5. Cross Section Data Evaluation

The cross section evaluation for natural copper and its two principle isotopes was completed. Various ENDF/B checking codes were used to check and correct the data files for copper. Following a final check, which included the automated plotting of the pertinent ENDF/B data files, the data was sent to the National Neutron Data Center at BNL for distribution. A topical report, AI-AEC-12741 was released.

C. DOCUMENTATION

The following reports were issued during FY 1969.

"Storage of Microscopic Cross Section Data in the AIENDF," NAA-SR-11980, Vol II (July 1968)

"Atomics International Reactor Computational System," AI-AEC-MEMO-12735 (August 1968)

"Evaluated Neutron Cross Sections for Copper-63, Copper-65, and Natural Copper," AI-AEC-12741 (December 1968)

"B"/360 GRISM Input Description," AI-AEC-12271 (January 1969)

"SCORE II, An Interactive Neutron Evaluation System," AI-AEC-12757 (March 1969)

"TYCHE IV and Auxiliary Programs for the S/360," AI-AEC-TDR-12828 (May 1969)

"Program EMDFAI, Cross Section Format Conversion from ENDF/B to AIENDF," AI-AEC-TDR-12827 (May 1969)

"Neutron Scattering from Nonspherical Nuclei," Phys. Rev. 177, 1395 (January 1969)

The following paper was presented during FY 1969:

"Comparison of Analysis of Fast Critical Assemblies Using Several Cross Section Data Sets and Different Cross Section Processing Codes," International Conference on the Physics of Fast Reactor Operation and Design, London, England (June 1969)

III. EVALUATION OF EFFORT DURING FY 1969

To overcome deficiencies in, and enhance the utilization of current evaluation methods, a comprehensive automated system is being developed to encompass all the operations from the generation of new data to the evaluation of final cross section libraries. Such an extensive undertaking has been made possible by major technological advances in the new generation of computers. In particular, these advances are represented by new devices which permit on-line communication between man and a high speed digital computer. With such devices it is possible for a decision to be made during the execution of a problem which will influence the final result. The SCORE program is representative of such a man - computer interactive system.

The recoding and optimizing of the SCORE program to allow execution in a core memory of approximately 180,000 bytes eliminated a major objection of too large a core storage, thus allowing for wider program utility. In the process

of recoding to create the present overlay structure many former coding inefficiencies were eliminated and the presentation of information for many options improved.

The rewriting of all SCORE related graphics subroutines, originally written in machine language, into Fortran has effectively eliminated the dependence of the program on machine language routines except for the basic graphics support package. An overall result is that, for the data evaluator, the case with which he can utilize SCORE has been enhanced.

The interactive graphics computer code SCORE II was released for general distribution. It is anticipated that the general availability of this program will produce an increase in the number of computer graphics related applications. The SCORE program was made operational at the AWRE, Aldermaston. An exchange with AWRE has been established, by which they will contribute computer code subroutines for the production of hard copy and automatic spline fitting for the succeeding version of SCORE. The utilization of SCORE has been furthered through the establishment of cooperative programs with Idaho Nuclear and the University of Illinois in areas of resonance data evaluation and with the National Neutron Data Center at Brookhaven in the area of cross section data retrieval, testing, and display.

To aid in the testing of ENDF/B microscopic nuclear data, an extremely fast running Monte Carlo code, which computes the neutron age and higher moments, by means of recursive relations was reactivated, modified, and improved. This code, TYCHE IV, was used to economically evaluate cross section data from the ENDF/B data files. Based on results from TYCHE IV calculation, recommendations for the reevaluation of the total and elastic scattering cross section data for carbon and deuterium were forwarded to the MNDC at Brookhaven.

Results obtained thus far in the Phase II 'benchmark' criticals data testing illustrate variations in multigroup constants and fluxes. The reasons for these variations are not fully understood and may prove detrimental to present and future CSEWG Phase II data testing.

Program:	General Reactor Technology
AEC Task:	26-C, Reactor Physics Measurements
Project Manager:	H. A. Morewitz
Reporting Period:	Fiscal Year 1969
General Order: 7762	Subaccount: 13210 AEC Category: 04-40-01-02.1

Principal Investigator: R. K. Paschall

I. PROJECT OBJECTIVES

The purpose of the fast reactor physics program is to supply data pertinent to the safe and economic, design and operation of fast power reactors. Safety and economics often compete in good reactor design, and very conservative estimates are usually made in the area of safety because of the paucity of precise physics data. This program is designed to study these specific areas, and to confirm the nuclear parameters and calculational methods used on conceptual evaluation and preliminary design.

The large volume of coolant (50%) and structural material (15%) in current fast reactor design make increasingly important the accurate knowledge of light element scattering cross-sections which affect the magnitude of both the Doppler and sodium-void effects. Also of concern is the resonance shielding for various mixtures of the light elements.

A series of integral experiments are being performed by use of coolant material (sodium) and the predominant structural material (iron). The measurements seek to determine the differential neutron spectrum in large volumes of sodium, in a large quantity of pure iron, and in appropriate mixtures of these materials, for both isotopic and reactor neutron sources. The resulting neutron spectra will be compared to those predicted on the basis of Monte Carlo calculations, in order to check the scattering cross sections presently used. The use of a reactor as a neutron source will allow, in addition, reactivity measurements of the sodium void and direct studies of spectral changes occurring during this voiding. The objectives of this project correspond to those of Task 9-2.11 of the LMFBR Program Plan, Section 9 (WASH-1109).

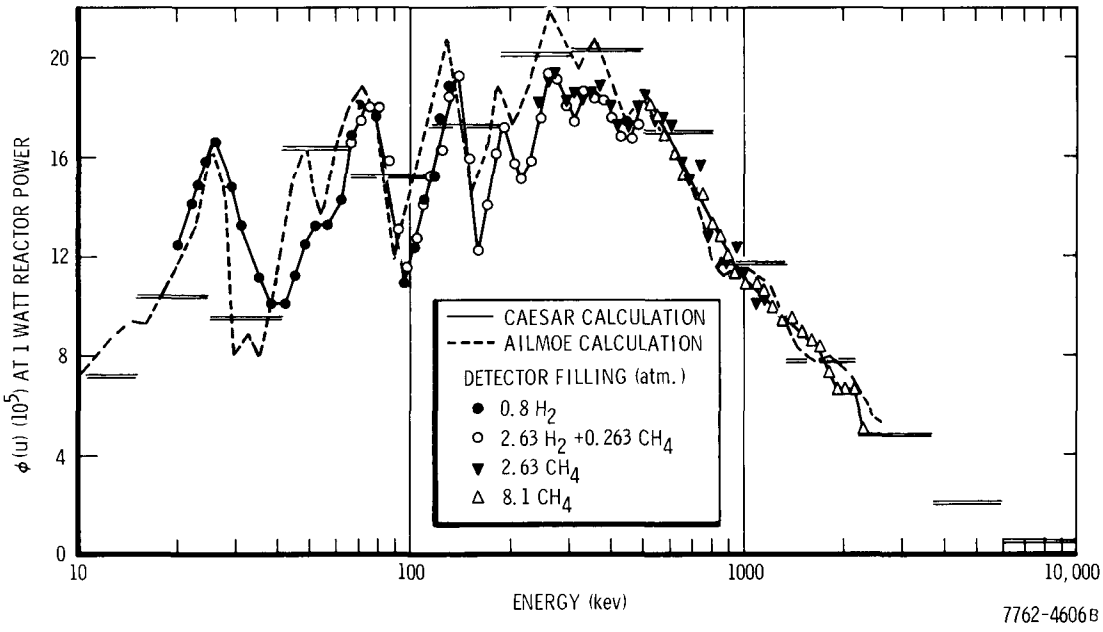

Figure 1. Neutron Spectrum in Center of ECEL Reactor Core 17

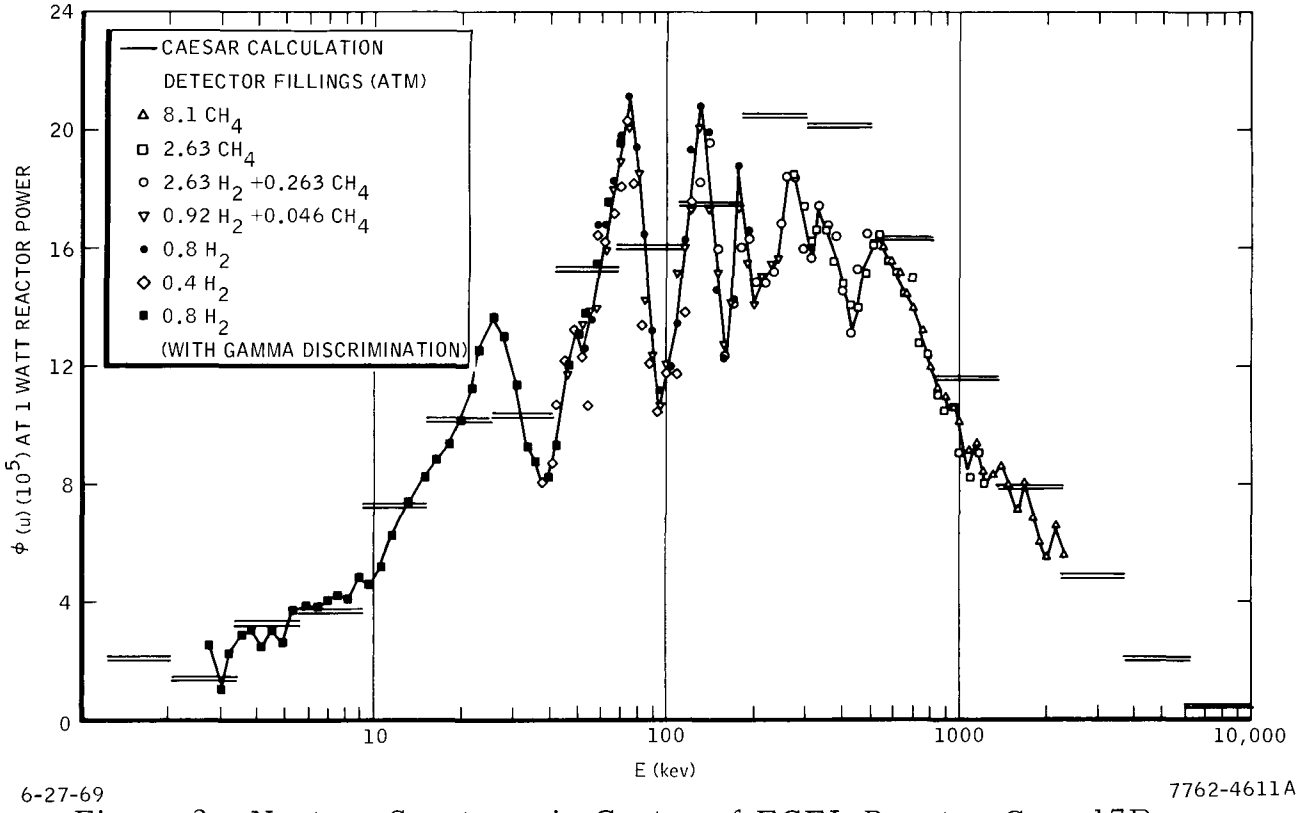

Figure 2. Neutron Spectrum in Center of ECEL Reactor Core 17P

II. TECHNICAL PROGRESS DURING FISCAL YEAR 1969

A. NEUTRON SPECTRA IN THE ECEL REACTOR

Neutron spectrum measurements, using proton-recoil detectors, were made in the ECEL reactor Cores 17 and 17P. A topical report AI-AEC-12855, is being issued describing the details of the measurements and comparing them with calculated spectra. Figure 1 shows the measured and calculated spectrum in the center of Core 17. Core 17P was made from Core 17 by replacing a central subzone of the test region with pin-type fuel elements. The spectrum in the center of 17P is shown in Figure 2. The measured spectra in both cores are compared in Figure 3. A specific difference was noted at 440 kev where the extra oxygen in the pin-type fuel ($U^{238}O_2$) of 17P caused a strong flux depression. Also, the extra aluminum in the fuel pins (35 wt % fully enriched uranium in aluminum alloy) caused higher peaks and deeper valleys in the flux below 100 kev. Generally, good agreement was obtained between the measured and calculated results.

Figure 4 shows the Core 17 spectrum measured with detectors located outside the reactor and looking at a beam of neutrons from the core center. It is

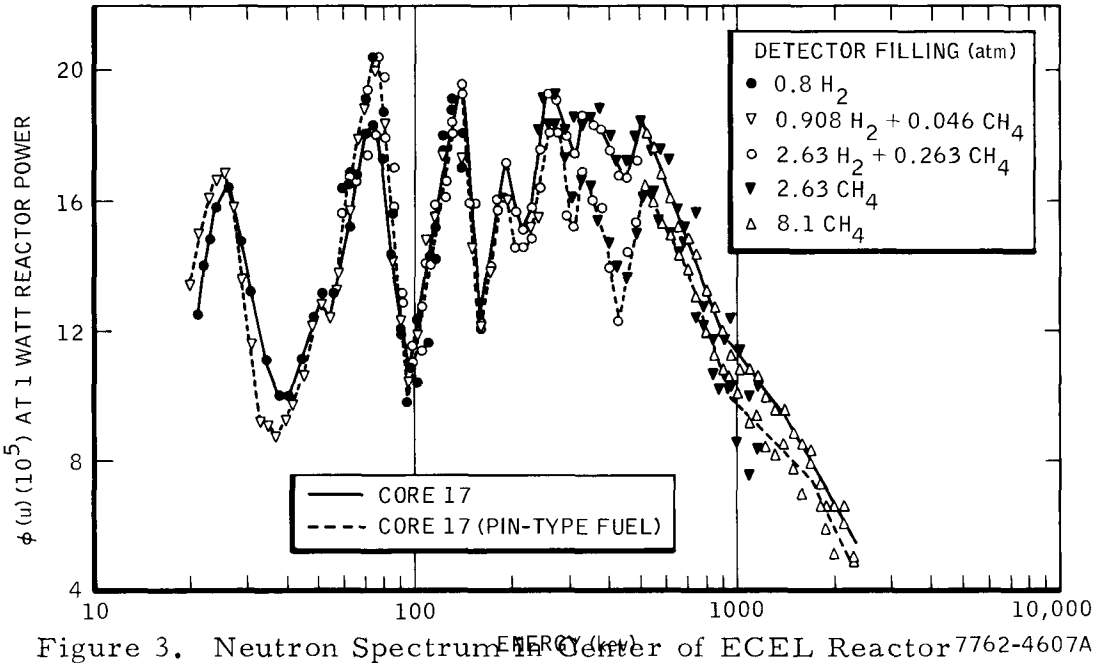

Figure 3. Neutron Spectrum in Center of ECEL Reactor Cores 17 and 17P

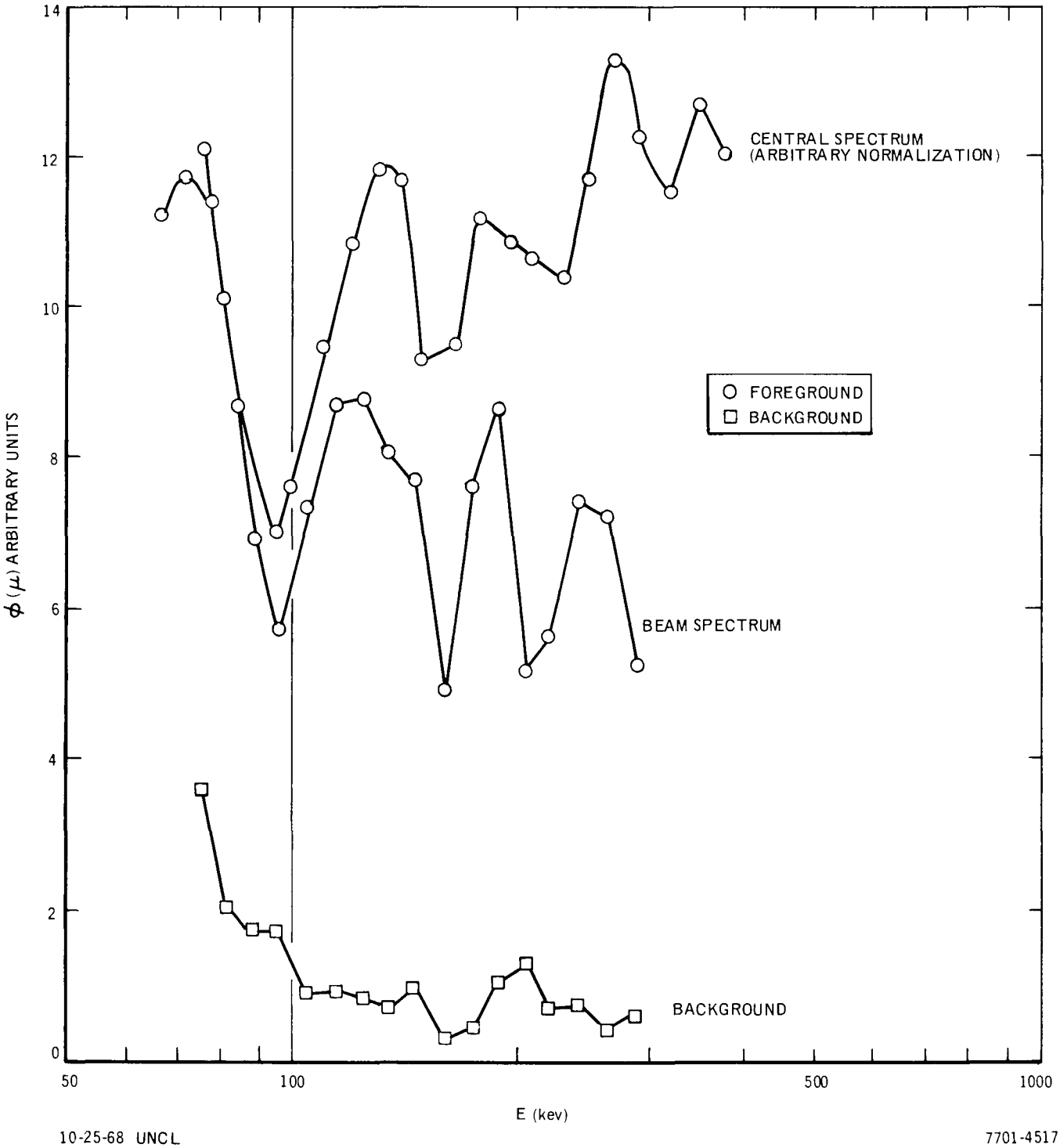

Figure 4. Neutron Spectrum in Center of ECEL Reactor Core 17 Measured With Detector Outside of Reactor

normalized and compared with the spectrum measured by detectors in the test region. Only a limited energy range was observed with the detectors outside, since those measurements were of an investigatory and preliminary nature; nevertheless, both sets of data agree quite well.

Some results (at selected energies) of spectra measurements made at 2-in. intervals along a radius in Core 17P are shown in Figure 5. The data at 14 in. from the center of the test region were taken with the detector slightly in the driver region.

The neutron spectrum was also measured in Core 18 which is similar to Core 17, except all the stainless steel cans filled with sodium in Core 17 are replaced by empty cans. The results of data analysis are shown in Figure 6. A cadmium-covered foil package (Al, Co, Cu, In, and S) was placed at the center of the test region; another was placed 5 in. off center and exposed for 4 hr at 150 watts. It is hoped that some approximate integral fluxes can be measured in this manner. Data reduction remains to be completed.

B. NEUTRON SPECTRA IN SODIUM AND STEEL

The first series of neutron spectra measurements in a large volume of sodium were completed for the Reactor Physics Measurements program. Data were taken from a few ev to 300 kev with proton-recoil detectors. The experimental arrangement is shown in Figure 7. There was no shielding around the sodium to prevent neutrons from entering the sides of the sodium after scattering off the walls of the test room. The measured spectra are shown in Figure 8 together with calculated results. The influence of wall return background was very large in the ninth sodium slab.

Following those measurements, neutron spectra were measured in several arrangements of sodium and stainless steel for the FFTF shielding program (Task 24b). The experiments are described in detail in Report AI-AEC-MEMO-12838. In all the arrangements, shielding was placed around the sodium and steel to reduce the wall return background. In the first arrangement, steel was positioned to follow nine slabs of sodium. Data were taken in the ninth sodium slab and first iron slab. The results are shown in Figure 8. The wall return background was still so large that the arrangement was modified to five

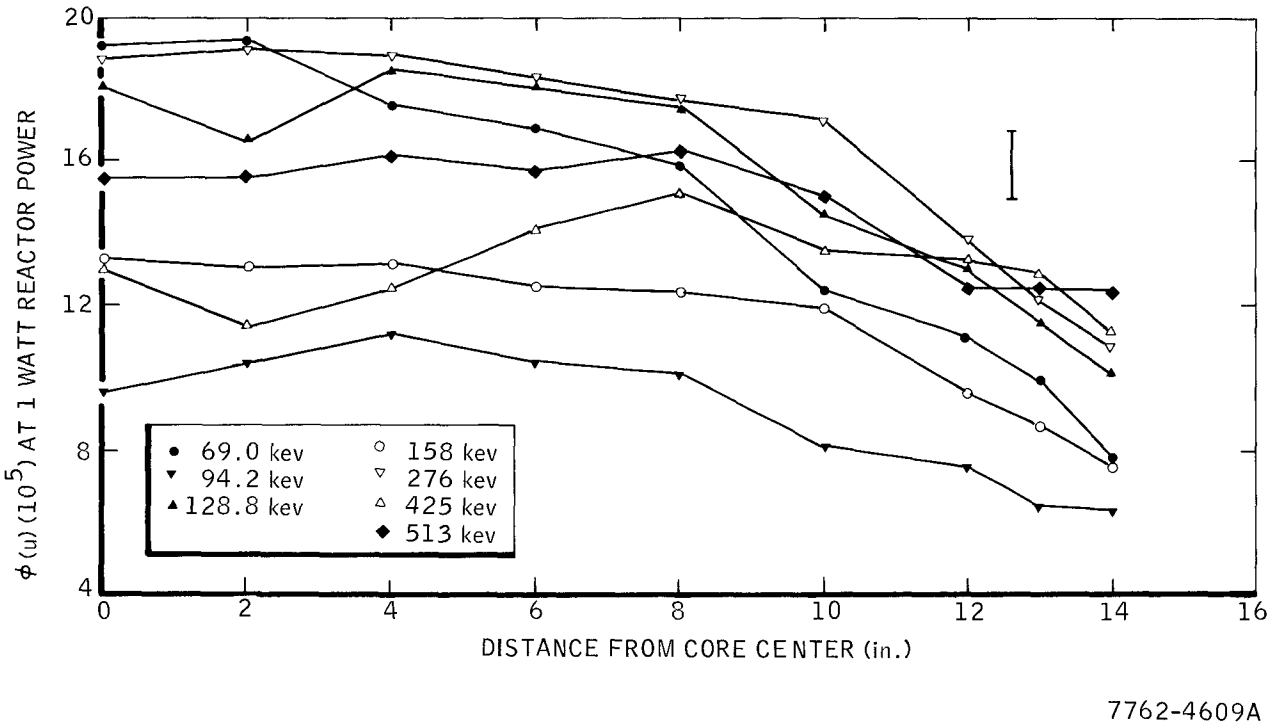

Figure 5. Radial Flux Measurements in ECEL Reactor Core 17P

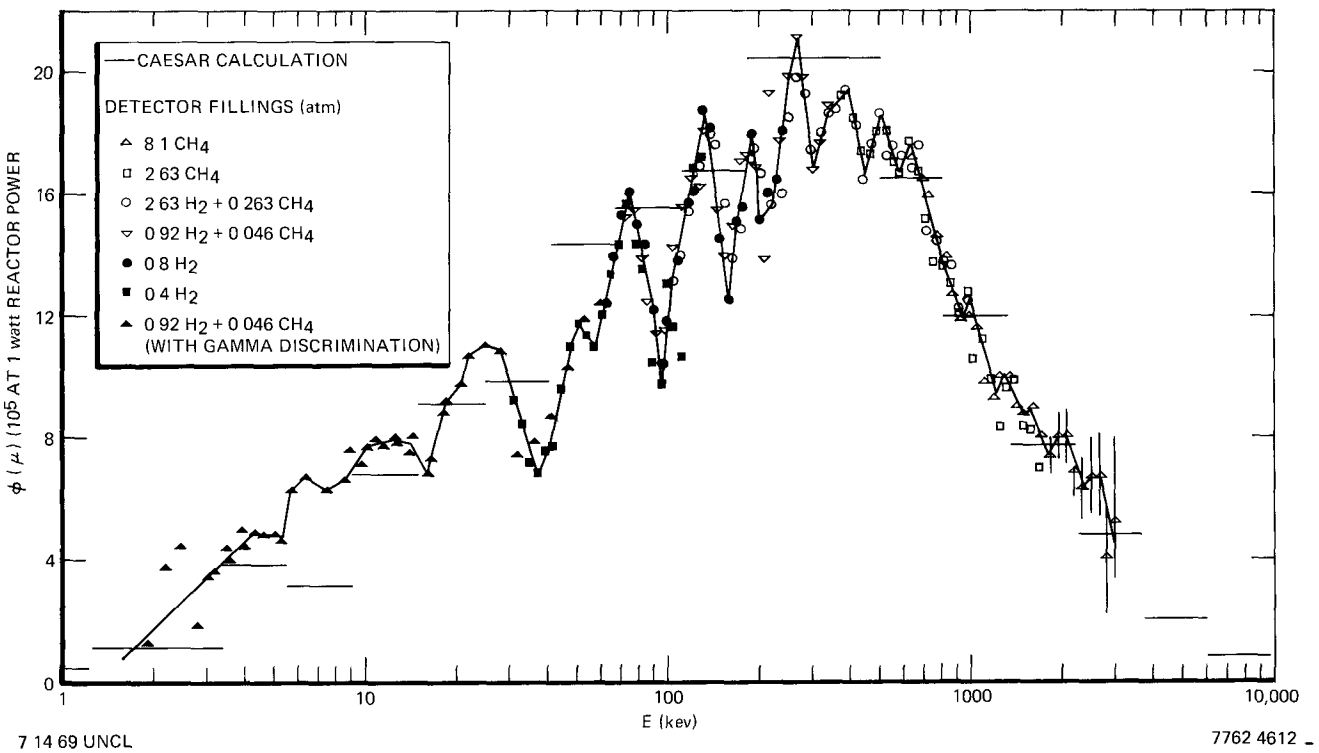

Figure 6. Neutron Spectrum in Center of ECEL Reactor Core 18

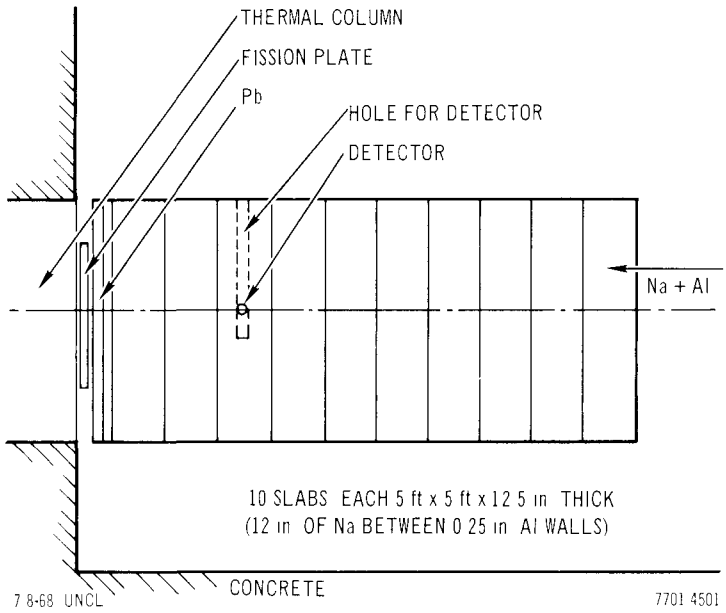

Figure 7. Experimental Arrangement for Shielding Measurements in Sodium

sodium slabs followed by steel. Figure 9 shows the spectra measured in this arrangement together with calculated results which agreed very well. A paper, "Neutron Spectra Measurements in Sodium and Stainless Steel," by R. K. Paschall was presented at the November 1968 American Nuclear Society Meeting in Washington, D. C. This paper described the first series of sodium measurements and the arrangements of sodium followed by steel.

The next arrangement of sodium and steel is shown in Figure 10. The measured and calculated results are shown in Figure 11. The placement of extra shielding to remove wall return background is shown in Figure 12. In order to check the effectiveness of this extra shielding, the sodium slab centered at 89.7 cm from the fission plate was replaced with LiH slabs (removing nearly all the neutrons coming directly from the fission plate and the spectrum was remeasured at 142.4 cm from the source. The wall return background was thus determined to be only about 1% of the direct flux.

The final arrangement was a repeat of the ten sodium slabs only. Shielding against wall return background was used, and data was taken from a few kev up to 2.3 Mev. The results are shown in Figure 13. In this case, a

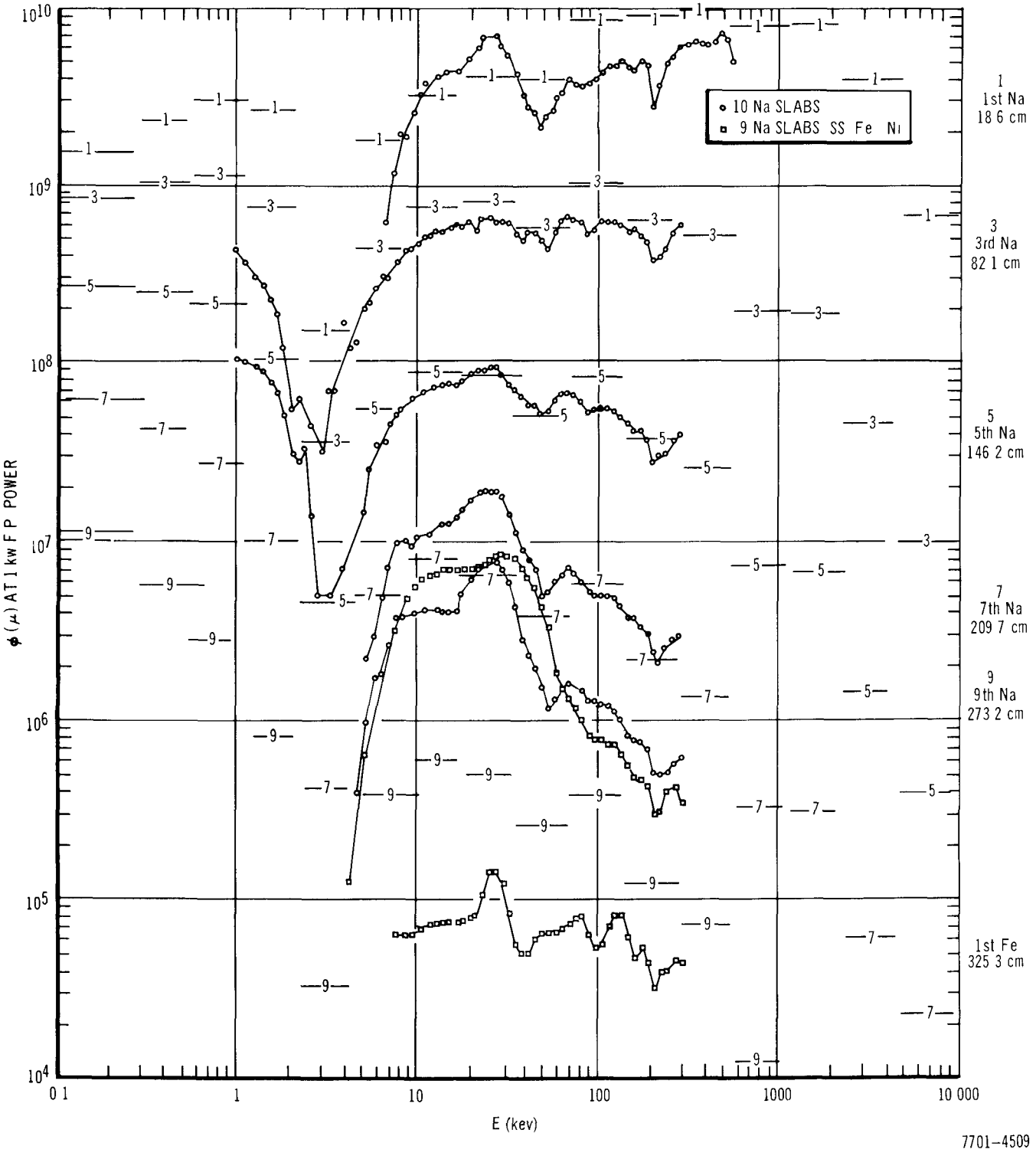

Figure 8. Neutron Spectra in First Series of Sodium Measurements

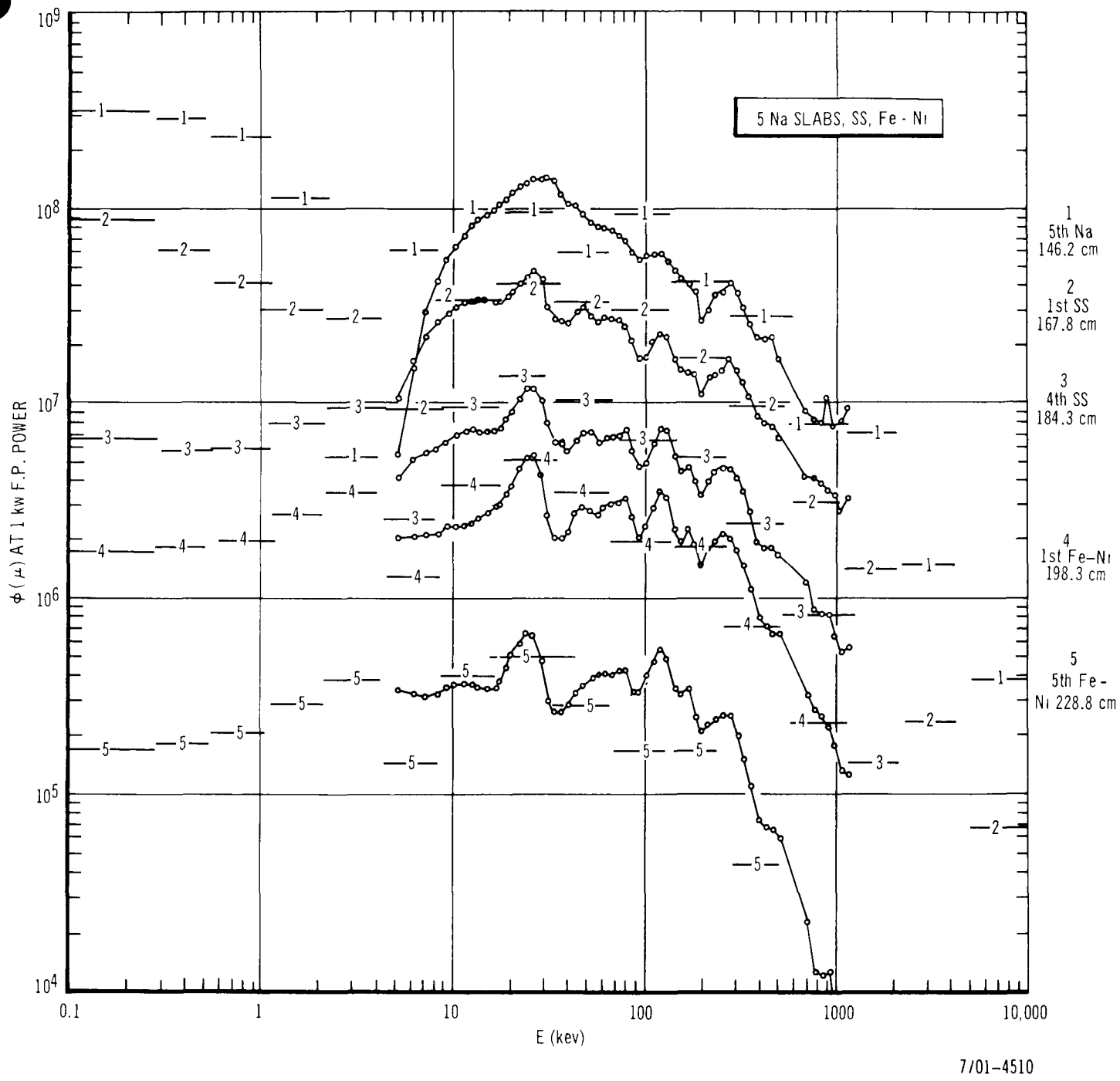

Figure 9. Neutron Spectra Measured in 5 Sodium Slabs Plus Steel Shield

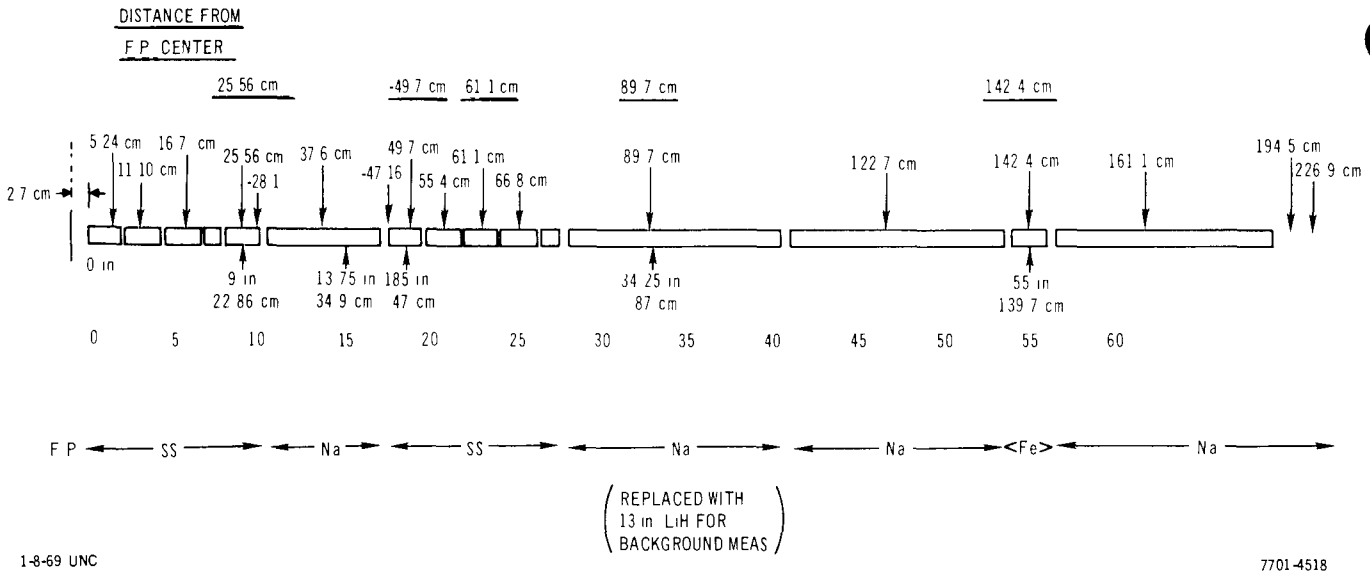

Figure 10. Radial Shield Configuration of Sodium and Steel

considerable fraction of wall return background (compared to the small direct flux) still penetrated the shield to influence the data in the ninth sodium slab; however, by measuring the amount of wall return, an approximate correction could be applied to the data when determining sodium attenuation curves.

An additional measurement was that of the spectrum at the center of the fission plate with the thermal column on one side and nothing on the other side; thus, the actual spectrum of neutrons striking the sodium and steel volumes was determined. Figure 14 shows that the measured spectrum agrees with the calculated spectrum but differs considerably from a pure fission spectrum.

In order to verify the feasibility of making shielding measurements with some shielding material next to the STIR reactor (i.e. by replacing the graphite in the thermal column with shielding material), the neutron spectrum was measured close to the reactor. A 7-in. thick window of Bi and Pb separates the reactor from the graphite thermal column. A 4-in. square graphite log was removed from the center of the thermal column and the proton-recoil spectrometer was inserted to where the detector center was 5 in. from the Bi, Pb window. The spectrum at that point is shown in Figure 15. An ANISN calculation is also shown, approximately normalized to the measured results below 500 kev. The measured and calculated results agree very well over the

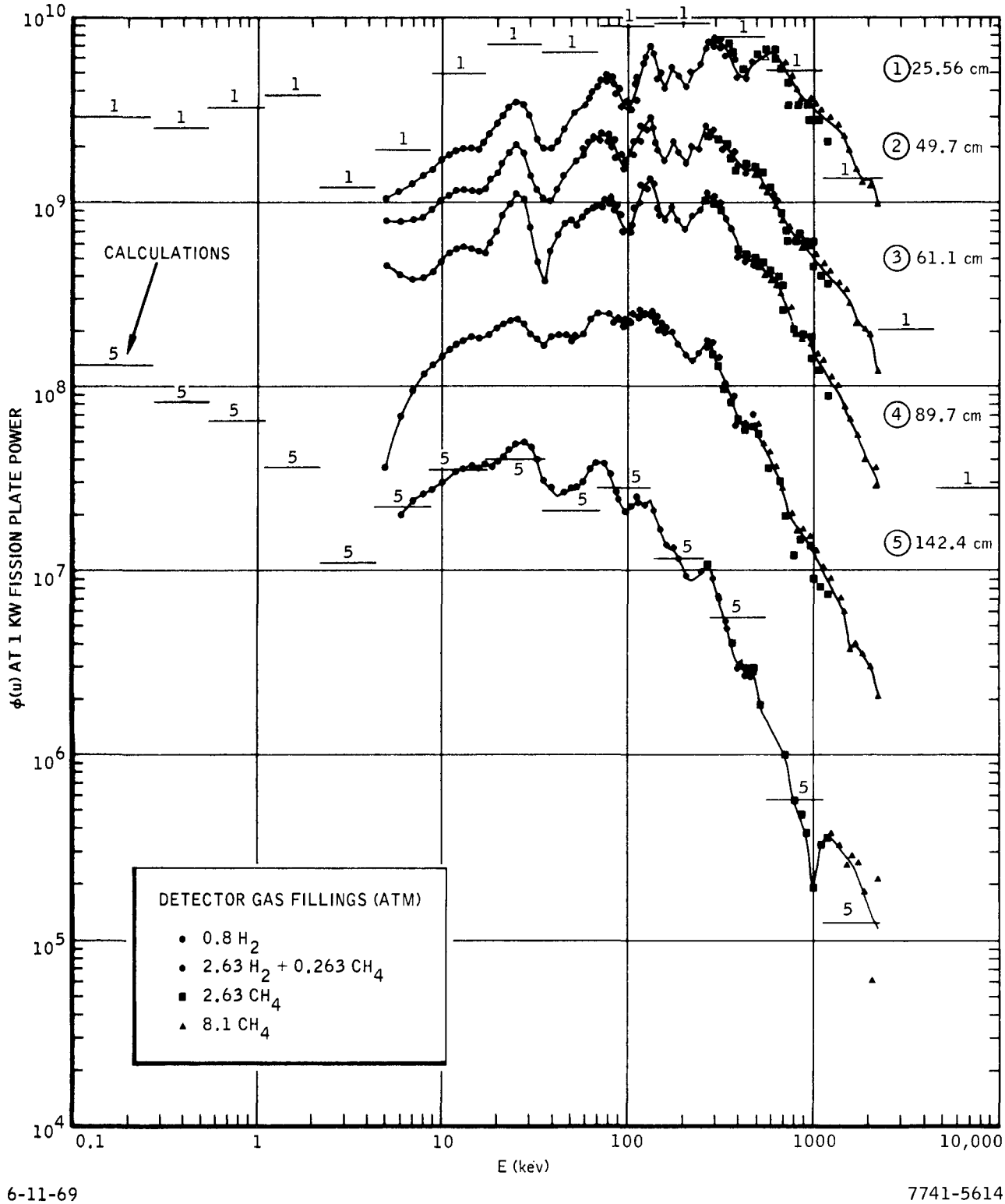

Figure 11. Neutron Spectra in Radial Shield Configuration

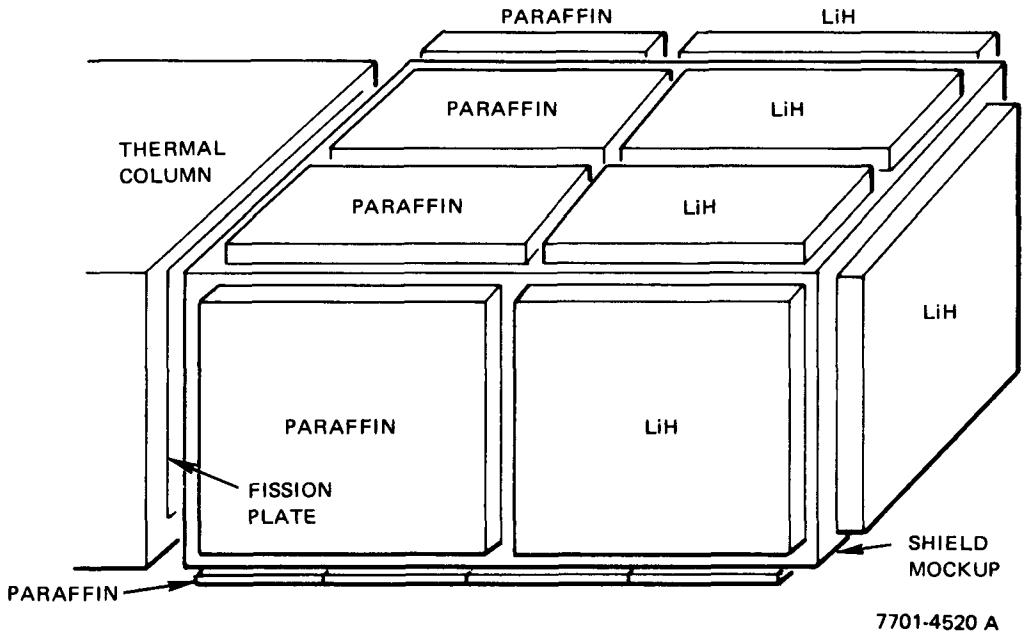

Figure 12. Placement of Shielding to Remove Room Return Neutron Background

entire energy range of the measurements. Additional ANISN calculations were made for 13 ft of sodium around the STIR reactor and for 13 ft of sodium around a fast reactor. The STIR reactor calculation was made for both a 7-in. gap between the reactor and sodium (as actually caused by the Bi-Pb window) and for a 37-in. gap to put the sodium volume at the same distance from the reactor center as in the fast reactor calculation. Those results are now being evaluated.

III. EVALUATION OF EFFORT DURING FY 1969

Considerable data were taken with the proton-recoil neutron spectrometer system. This included both measurements in the fast test region of the ECEL reactor and shielding measurements in large volumes of sodium and steel for the FFTF shielding program. During this period, the use of proton-recoil detectors with high pressure fillings of methane and hydrogen extended the measurable energy range up to approximately 2.3 Mev. The computer code to analyze the data (written by P. W. Benjamin, et al, AWRE Report No. 09/68) was modified to include nitrogen in the filling gas since about 5% nitrogen is added to many of the detectors for use in energy calibration. Several minor

errors in the code were corrected. (These omissions and errors were the cause of several puzzling anomalies which had consistently appeared in previous spectral results.) Another modification extends the upper range for data analysis on each detector so that the maximum energy may now be as high as 4.0 Mev.

The low energy range of the detectors still needs improvement. Even though data were taken down to a few kev (using two-parameter gamma discrimination), the effort to reduce the data was long and tedious. Also, systematic errors were quite large. Part of the problem was in the existing electronic circuitry and part was due to not having an on-line computer (or at least a hard-wired divide circuit) to aid in analysis of the two-parameter data. The circuitry problems have been (or will be shortly) solved and corrected.

Generally good agreement was obtained between measurements and calculations in the ECEL reactor cores. There are some energy groups where it appears that the calculations need improving, either in the geometrical approximations or cross-section data (raw data or group averaging methods). Measurements using a reentrant tube to the core center appear very promising.

The measured and calculated attenuation curves in sodium and sodium-steel mixtures agreed quite well. Some anomalies arose when lead was placed between the eighth and ninth sodium slabs and repeat data were taken in the center of the ninth slab. Other experiments show little effect due to lead shielding; therefore, these questionable effects need further investigation in shielding measurements. Additional data are needed beyond the nine feet of sodium of previous measurements to improve confidence in extrapolating through thicker shields. Also, more shielding is required around the sodium to reduce room return background more effectively at the greater distances. In conjunction with these measurements, transport theory calculations in two dimensions should be made to improve geometrical approximations to the actual experiments.

The spectrum measurements made near the center of the fission plate indicate that a true fission spectrum is not impinging upon the shielding materials; however, the calculation made with graphite next to the fission plate agreed with the experiment. This suggests that more accurate shielding calculations can be made by starting with correct source geometry.

Most of the work accomplished this year is summarized and detailed in Reports AI-AEC-12855 (ECEL experiments), AI-AEC-MEMO-12838, and Transactions of the ANS, November 1968 (FFTF shield experiments).

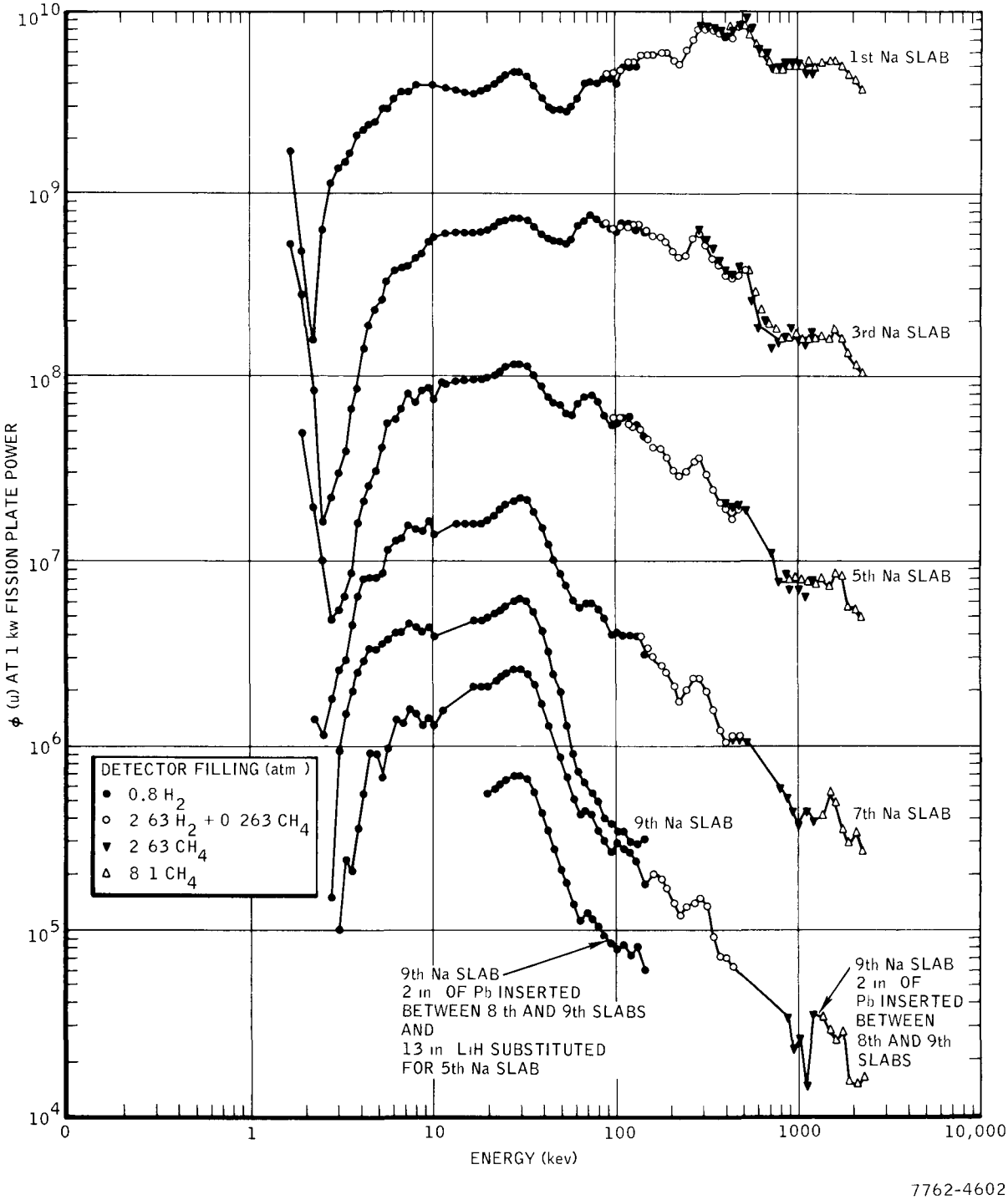

Figure 13. Neutron Spectra in Second Series of Sodium Measurements

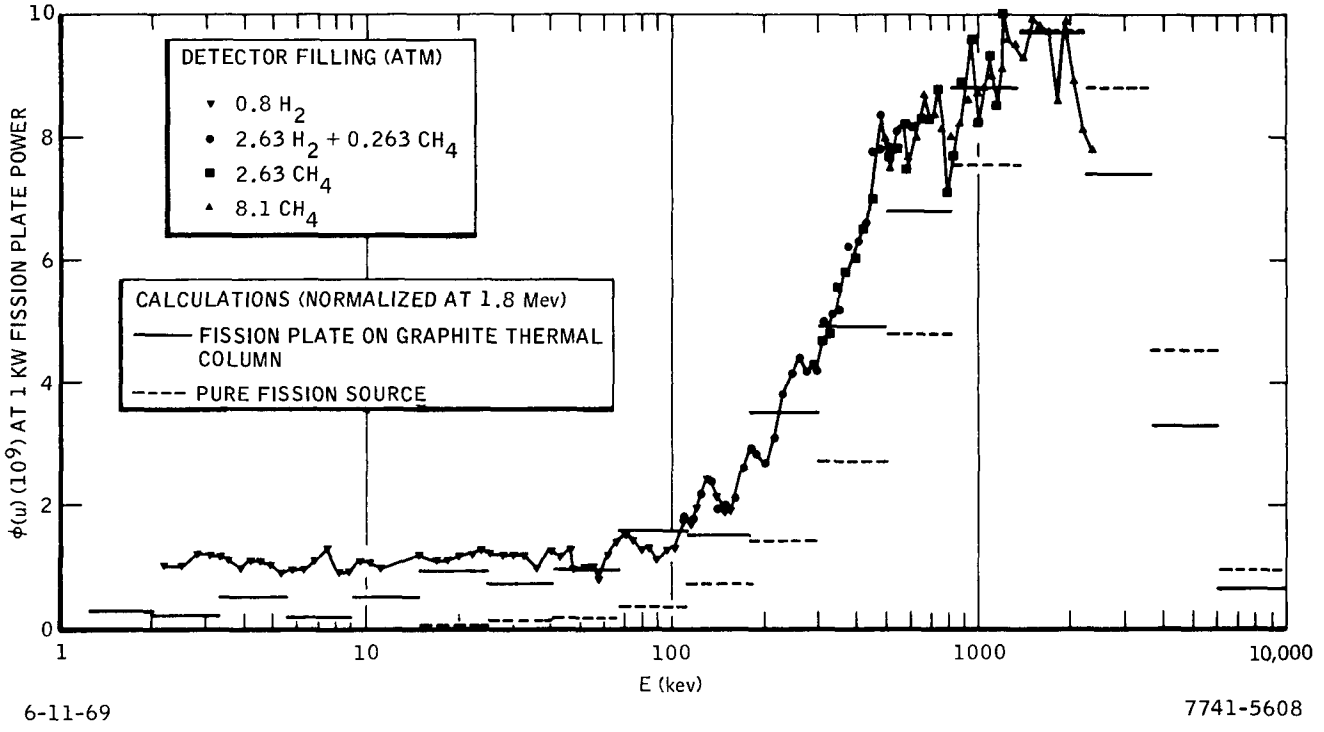

Figure 14. Neutron Spectrum at Center of Fission Plate

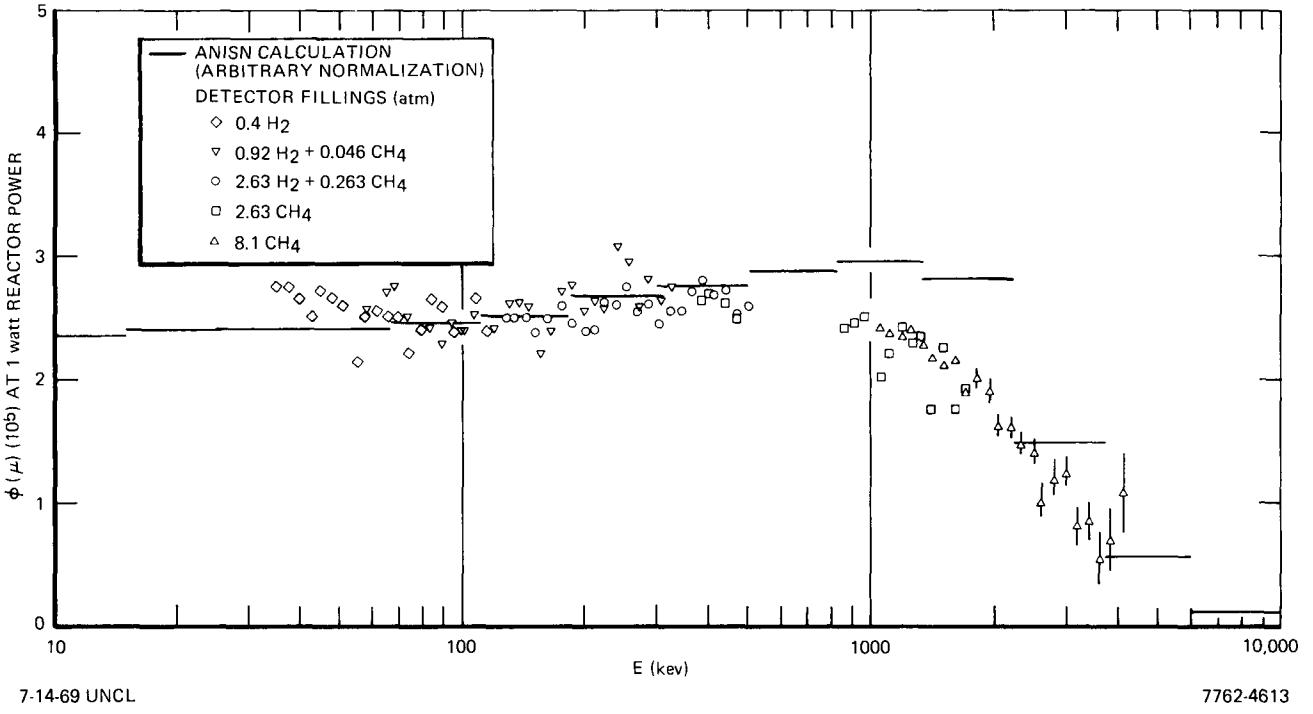

Figure 15. Neutron Spectrum in STIR Facility Thermal Column (5 in. from BI window)